Efficiently assessing the early-age cracking risk of cementitious materials with a mini temperature stress testing machine

Liang, Minfei; Chang, Ze; Holthuizen, Patrick; Chen, Yu; He, Shan; Schlangen, Erik; Šavija, Branko

DOI
10.1016/j.cemconcomp.2024.105710

Publication date
2024

Document Version
Final published version

Published in
Cement and Concrete Composites

Cement and Concrete Composites 153 (2024) 105710

Contents lists available at ScienceDirect

Cement and Concrete Composites

journal homepage: www.elsevier.com/locate/cemconcomp

Efficiently assessing the early-age cracking risk of cementitious materials with a mini temperature stress testing machine

Minfei Liang [a], Ze Chang [a,b,*], Patrick Holthuizen [a], Yu Chen [a], Shan He [a], Erik Schlangen [a], Branko Šavija [a]

[a] Microlab, Faculty of Civil Engineering and Geosciences, Delft University of Technology, Delft, 2628, CN, the Netherlands
[b] Department of Mechanical Engineering, Eindhoven University of Technology, Eindhoven, 5600MB, the Netherlands

ARTICLE INFO

Keywords:
Early-age cracking
Temperature stress testing machine
Elastic modulus
Autogenous deformation
Creep/ relaxation

ABSTRACT

Temperature Stress Testing Machine (TSTM) is a universal testing tool for many properties relevant to early-age cracking of cementitious materials. However, the complexity of TSTMs require heavy lab work and thus hinders a more thorough parametric study on a range of cementitious materials. This study presents the development and validation of a Mini-TSTM for efficiently testing the autogenous deformation (AD), viscoelastic properties, and their combined results, the early-age stress (EAS). The setup was validated through systematic tests of EAS, AD, elastic modulus, and creep. Besides, the heating/cooling capability of the setup was examined by tests of coefficient of thermal expansion by temperature cycles. The results of EAS correspond well to that of AD, which qualitatively validates the developed setup. To quantitatively validate the setup, a classical viscoelastic model was built, based on the scenario of a 1-D uniaxial restraint test, to predict the EAS results with the tested AD, elastic modulus, and creep of the same cementitious material as the input. The predicted EAS matched the testing results of Mini-TSTM with good accuracy in 6 different cases. The viscoelastic model also provided quantitative explanations for why variations in early AD do not influence the EAS results. The testing and modelling results together validate the developed Mini-TSTM setup as an efficient tool for studying early-age cracking of cementitious materials. At the end, the potential limitations of the Mini-TSTM are discussed and its applicability for concrete with aggregate size up to 22 mm is demonstrated.

1. Introduction

Early-age cracking (EAC) is a significant problem in the construction of concrete structures. When the early-age shrinkage (e.g., thermal, autogenous, and drying shrinkage) is restrained, tensile stress accumulates and EAC happens if the tensile stress exceeds the tensile strength of concrete, leading to economic issues for the contractors and degrading the durability of the concrete structures. A proper setup for testing the early age stress (EAS) evolution is essential for assessing the EAC potential and preventing EAC problems.

Many experimental setups have been proposed for testing the EAS evolution, including the rigid cracking frame test [1], ring test [2,3], internal restraint test [4], and temperature stress testing machine (TSTM) test [5,6]. Among these testing methods, the TSTM stands out with advantages in explicit and flexible mechanical loading schemes, active temperature control, and tunable restraint degree [7]. With TSTM, a broad range of parameters can be studied, including different temperature profiles, mixtures, creep/relaxation, and shrinkage on the EAS evolution. Such parametric studies are important for understanding EAC problems and developing numerical models for predicting EAS evolution. The EAS is a complex result of environment, mixture, material behaviors, and material properties, as shown in Fig. 1. Based on the concrete behaviors and properties (tested by TSTMs) corresponding to a certain mixture and environmental condition, the evolution of EAS in restrained concrete structures can be calculated by analytical or finite element (FE) approaches based on a viscoelastic mechanical model or thermo-chemo-mechanical framework [8–12]. Therefore, the TSTM is a powerful tool not only for testing the EAS itself but also for laying the basis for developing modeling techniques of EAS evolution.

* Corresponding author. Microlab, Faculty of Civil Engineering and Geosciences, Delft University of Technology, Delft, 2628, CN, the Netherlands.
E-mail addresses: M.Liang-1@tudelft.nl (M. Liang), Z.Chang@tue.nl (Z. Chang), P.E.Holthuizen@tudelft.nl (P. Holthuizen), Y.Chen-6@tudelft.nl (Y. Chen), S.He-2@tudelft.nl (S. He), Erik.Schlangen@tudelft.nl (E. Schlangen), B.Savija@tudelft.nl (B. Šavija).

https://doi.org/10.1016/j.cemconcomp.2024.105710
Received 15 May 2023; Received in revised form 31 May 2024; Accepted 9 August 2024
Available online 10 August 2024

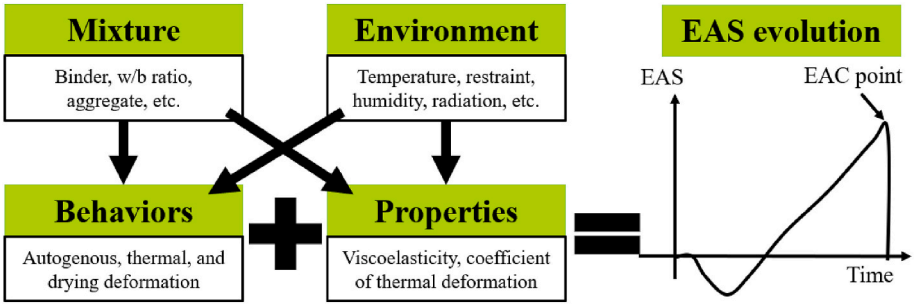

Fig. 1. Schematic diagram of EAS evolution.

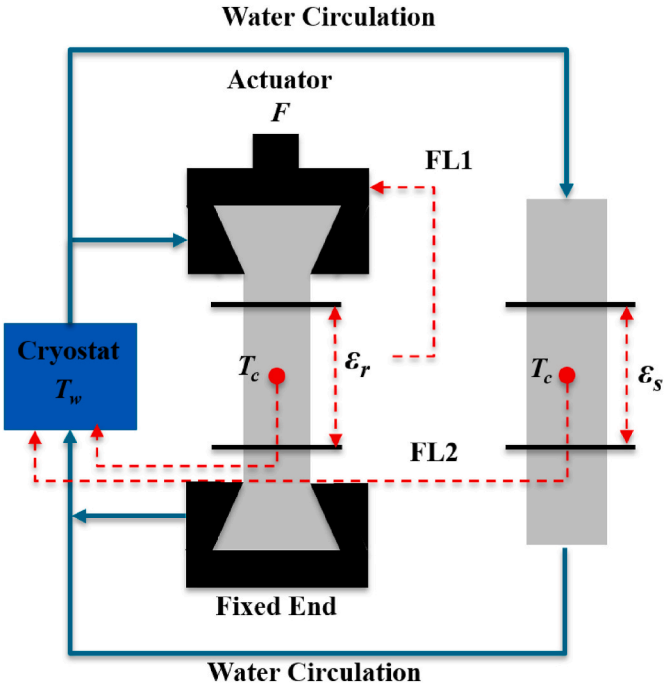

Fig. 2. Schematic diagram of a TSTM system.

1.1. General design of TSTM

A typical TSTM system can measure the EAS evolution of a restrained dog-bone specimen and the deformation of a free specimen, as shown in Fig. 2. In each specimen, 2 bars are embedded in the middle part to be attached with the Linear Variable Differential Transducers (LVDTs) used to measure the deformation of the middle part (i.e., ε_r and ε_s). The dog-bone specimen is fixed at one end and connected to an actuator and a load cell at the other end to apply a force, F. A set of cryostats, water pipes, and molds with embedded water channels is used to circulate water around the specimens and regulate the temperature therein. Two feedback control loops (FL1 and FL2) are used typically based on the proportional–integral–derivative (PID) controller. To fulfill the full-restraint condition, the value of the force F is determined by the feedback loop FL1 to fix the value of ε_r at 0. To make sure that the temperature in the specimen follows the pre-specified value, the feedback loop FL2 is used to adjust the temperature of water T_w according to the temperature in the specimen T_c measured by thermocouples. As an example, the TSTM system at the TU Delft is shown in Fig. 3.

1.2. Summary of representative TSTMs

In line with the basic design principles described in section 1.1, a number of TSTMs have been devised and applied in research related to the EAC of concrete. In Table 1, TSTMs from different institutes are compared in terms of specimen size, strain measurement, displacement control, and time-zero. All analyzed TSTMs use specimens longer than 1000 mm. The methods for measuring strain in the middle part of specimens differ the most among different TSTMs. The description in Table 1 about the strain measurement contains information on the location and number of LVDTs. For example, the strain measurement of TSTM at the TU Delft [14] is done by arranging 4 LVDTs at the two sides of the specimens. As for the control method to fulfill the full-restraint condition, most TSTMs (except the one at the TU Delft) control the force applied by the actuator using the stepping control method: if the deformation of the specimen exceeds a certain threshold, the actuator connected to the free end of the dog-bone specimen will apply a force to pull/push the specimen to its original position. In comparison, the TSTM at the TU Delft applies a PID controller to continuously fix the measured deformation at 0, which does not depend on the (arbitrary) threshold value. The selection of time-zero (i.e., the timing to start the test) also differs between different tests. Ideally, the time-zero should be set exactly after the placement of the fresh mixture. However, the selection of time-zero also depends on when the specimen is hardened enough to support the embedded bars. Criteria related to the stress level or setting time are often used to decide when the tests should be started.

The major concern of the existing TSTMs lie with their complexities and high cost. For each test, the process of pre-test installation, casting, and post-test disassembling is time-consuming and requires considerable manpower [19]. Existing TSTMs with a size typically longer than 1 m require more material and efforts. Taking the TSTM at the TU Delft as an example [14], a single TSTM test requires the teamwork of 3–4 people for 2 full working days (8 h per day) to cast 80 L of fresh material for 1 restrained specimen and 2 free specimens. As explained in Fig. 1, the EAS are the combined results of restrained deformation and viscoelastic properties. Correspondingly, the tests of autogenous deformation (AD), elastic modulus, creep, and EAS are required to develop a quantitative model of EAC assessment, which means the same mixture needs to be tested at least twice in the TSTM systems as in Fig. 2, neglecting the repeatability of each test. The high costs of TSTM tests hinder the use of such a powerful testing tool in understanding relevant mechanisms of the EAC of different cementitious materials, which is the main motive of this study to develop a more efficient version of this test setup.

Other concerns with the existing TSTMs are as follows:

1) In the TSTMs that use stepping control to provide full-restraint, the selection of threshold value is often subjective and can influence the testing accuracy [7,21].
2) The arrangement of LVDTs for strain measurement, which provides input for the feedback loop for the actuator (i.e., FL1 in Fig. 1), is often an issue that influences the credibility of the TSTM [21] and therefore a focus of recent studies on improved TSTMs [19,20]. Comparing the TSTMs listed in Table .1, some points have been made clear about the arrangement of LVDTs for strain measurement: 1) Instead of measuring the deformation at one side of the specimen, it should be measured at both sides to detect possible eccentric

Fig. 3. The TSTM at the TU Delft: (a) Setup for the restrained specimen; (b) Setup for the free specimen [13].

Table 1
Summary of representative TSTMs.

Source	Year	L*W*H (mm)	Strain Measurement	Control	Time-Zero
TUM [15]	1984	1500 *150*150	Two-side, 2 LVDTs	Stepping	Stress 0.01 MPa
Israel IT [16], Hohai U [6]	1990, 2015	1500*150*150	Free-end, 1 LVDT	Stepping	Stress 0.01 MPa
NTNU [17, 18]	1995, 2012	1000*88*100	Two-side, 4 LVDTs	Stepping	Initial setting
TU Delft [14]	2000	1450*150*100	Two-side, 4 LVDTs	PID	Setting time
UQ [19]	2018	1200*80*80	Top-side, 4 LVDTs	Stepping	Setting time
UTokyo [20]	2022	1200*120*120	Top-side 2 LVDTs at two ends before 24 h and two-side 2 LVDTs afterward	Stepping	Setting time

deformations; 2) Rather than measuring the deformation of the dog-bone specimen at the cross-head, it is favorable to measure the deformation at the straight part, where no stress concentration are present and therefore the result can be reliably used as input for numerical models; 3) The LVDTs should not be directly attached to the loading grip; otherwise, any slip between the loading grip and the specimen will also be included in the strain measurement, resulting in possible errors.

3) In most of the existing TSTMs, the specimens are tested horizontally, and friction may occur between the hardening specimen and the mold at the bottom. This may introduce further errors to the measured stress. Some measures to reduce the influence of friction were proposed, such as the use of Teflon sheets [19] and roller supports [20].

1.3. Significance of this study

In view of the main concerns of the existing TSTMs, we propose a lighter and smaller version of TSTM that can be more efficiently implemented while maintaining good testing accuracy. The design of the efficient Mini TSTM and testing procedures for different early-age material behaviors and properties is introduced in section 2. In sections 3 and 4, systematic validation schemes are designed to test the repeatability and reasonability of the mini-TSTM. Moreover, based on a viscoelastic model, the AD, elastic modulus, and creep compliance measured at different ages using the mini-TSTM are used to calculate the EAS in different cases. The good matches between the calculated EAS and that tested by the mini-TSTM directly validate the newly-designed setup.

2. The Mini-TSTM

2.1. Setup design

The new mini-TSTM should be simple and efficient. The overall design of the mini-TSTM is shown in Fig. 4. The total length of the specimen is 300 mm and the area of interest (i.e., the middle part of the specimen) is 50 × 50 × 100 mm^3 (Fig. 4(c)), which is significantly smaller than that of the TSTMs summarized in section 1.2. The small size of the Mini-TSTM enables direct installation of the setup into the Instron universal loading machine (see Fig. 4(b)), which is equipped with a load cell of 10 KN with an accuracy of 1 N. Therefore, the Mini-TSTM can be loaded vertically, which minimizes the influence of friction that can happen in horizontally loaded TSTMs (see section 1.2). Note that the section size of specimen 50 × 50 mm^2 will limit the maximum size of aggregate that can be used. However, this size is limited by the utilized loading machine, and can be increases if a more capable loading machine is available. The design of the AD testing machine (ADTM) is the same as the TSTM, except for the steel-made parts at two ends of the specimen. The test of AD by the Mini-ADTM is also conducted vertically, which reduces the influence of friction happening frequently in horizontal test. The design of Mini-TSTM/ADTM is introduced in the following aspects: 1) Mold, 2) Strain measurement, 3) Temperature control and 4) Assembly procedures.

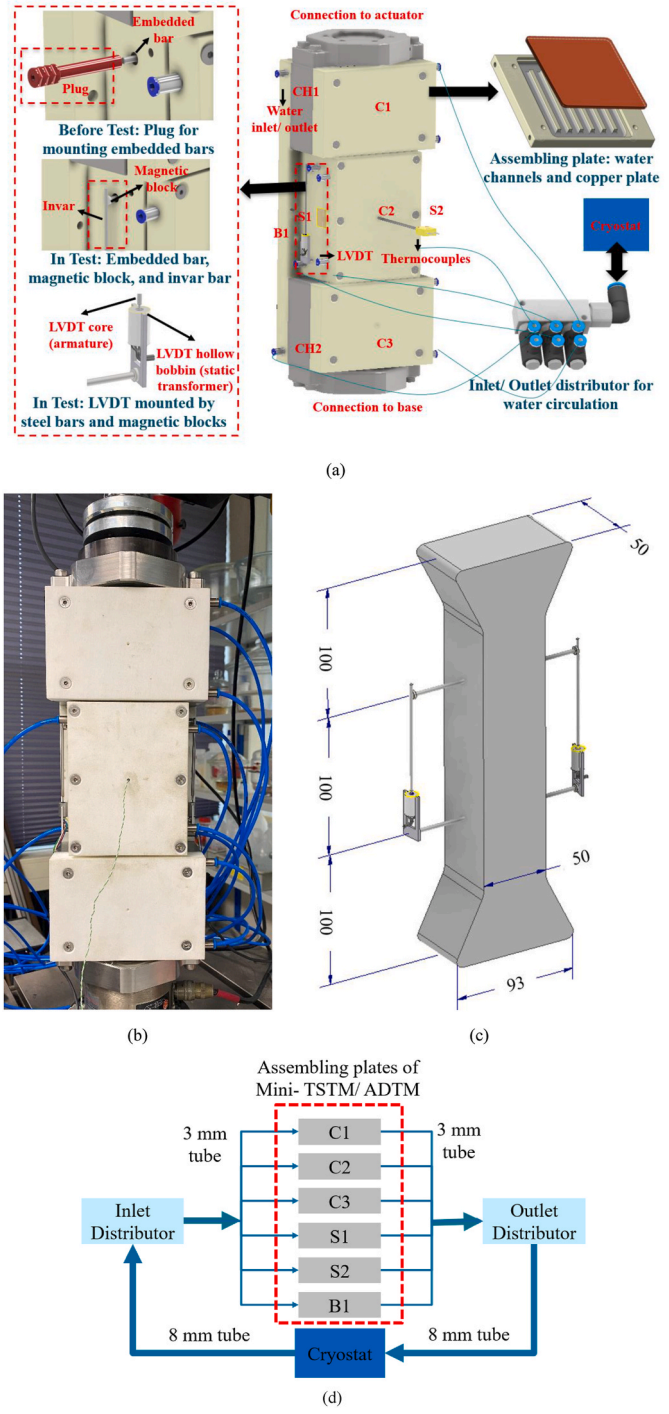

Fig. 4. The mini-TSTM: (a) overall design; (b) the efficient TSTM installed in the loading machine; (c) geometry of the dog-bone specimen (unit: mm); (d) parallel connection of water circulation system.

2.1.1. Mold

The mold of the Mini-TSTM is manufactured using Stereolithography (SLA) 3D printing with white powder-based polyamide (PA 2200), which is one of the most versatile 3D printing materials with good performance in strength, flexibility, and heat resistance. As shown in the middle of Fig. 4(a), the mold of the Mini-TSTM includes 3 covering plates (C1, C2, C3), 2 side plates (S1, S2), 2 crosshead plates (CH1, CH2), and 1 back plate (B1). In the Mini-TSTM, the plates CH1 and CH2 are made of steel, while in the Mini-ADTM the CH1 and CH2 are made by 3D printing with PA 2200. The assembly of all the plates is mainly by bolting. In each plate, except CH1 and CH2, water channels were designed and the inner surface of the plates in contact with the specimen is sealed with a copper plate (see upper right of Fig. 4(a)), which ensures good heat conduction and is therefore favorable for temperature regulation.

2.1.2. Strain measurement

The strain measurement of the Mini-TSTM and Mini-ADTM are both done by embedded steel bars, plastic plugs, LVDTs, invar bars, and magnetic blocks. The embedded steel bar has a length of 13.3 mm and diameter of 3 mm. As shown in the left of Fig. 4(a), before casting the fresh mixture in the mold, the embedded bar should be fixed by plugs (shown in red). Afterward, when the specimen is nearly hardened and the test is about to start, these plugs can be removed and the LVDTs can be attached to the embedded bars. The LVDT we used is an inductive displacement transducer that requires no contact during measurement. The LVDT is manufactured by Solartron Metrology and is composed of a hollow bobbin (static transformer) and a magnetic core (armature) (see the lower left of Fig. 4(a)). As the core travels in the hollow bobbin, the voltage changes are related to the displacement. The measurement range of the adopted LVDT is ±1 mm and the precision is 0.01 μm. The assembly of the strain measurement components can be seen in Fig. 4(c): first, the LVDT core should be glued to the lower side of the invar bar; then, with magnetic blocks as the connection, the upper side of the invar bar is attached to the upper embedded bar and the LVDT hollow bobbin is attached to the lower embedded bar. Thereby, the LVDT core can be set in the LVDT hollow bobbin to measure the deformation between the upper and lower embedded steel bars.

2.1.3. Temperature regulation

Temperature is regulated by circulating water in the plates C1, C2, C3, S1, S2, and B1. Each of these plates has water channels (Fig. 4(a) upper right) and a water inlet/outlet (Fig. 4(a) upper middle). As shown in Fig. 4(d), a parallel connection is used to circulate the water around the specimen: heated/cooled water is firstly pumped out from the cryostat to the inlet distributor, transported to each of the plates, and then sent back to the cryostat via the outlet distributor. The plastic water tubes, tube joints, water inlet/outlet, and distributors were manufactured by FESTO with a diameter of 3 mm and 8 mm. The thermocouple has an exposed welded tip (0.2 mm in diameter) and is produced by LABFACILITY with a measurement range of −75~250 °C and precision of 0.05 °C. Thermocouples are inserted into the middle of the specimen through the hole of plates C2 to measure the temperature inside the specimen. The temperature measured at plate C2, which is in the center of the specimen, is then set as the controlled objective of the temperature PID controller. Therefore, the water temperature of the cryostat can be continuously adjusted to ensure that the temperature at the center of the specimen follows the specified value.

2.1.4. Assembly procedure

The assembly of the Mini-TSTM and Mini-ADTM is shown in Fig. 5. Before the test, the plates CH1, CH2, S1, S2, and B1 should be firstly assembled by bolting to form the base mold. A layer of thin rubber (or plastic sheet) is laid on the inner surface of the mold to prevent leaking of fresh material. Then, the two embedded bars should be fixed in position by the plugs. Afterward, the specimen can be casted in the base mold, and another layer of rubber/plastic sheet is placed on top of the specimen. Then the plates C1, C2 and C3 are covered on top and fixed by bolts. Finally, the thermocouples are inserted into the fresh specimen and the water circulation systems are assembled by connecting all the water tubes and joints to control the temperature. Note that during all the procedures mentioned above, the specimen is still liquid and should be kept horizontally.

After a few hours (3–4 h in this paper, corresponding to the initial setting time of adopted cements), the Mini-TSTM and ADTM can be put vertically. The Mini-ADTM is placed freely, while the Mini-TSTM is

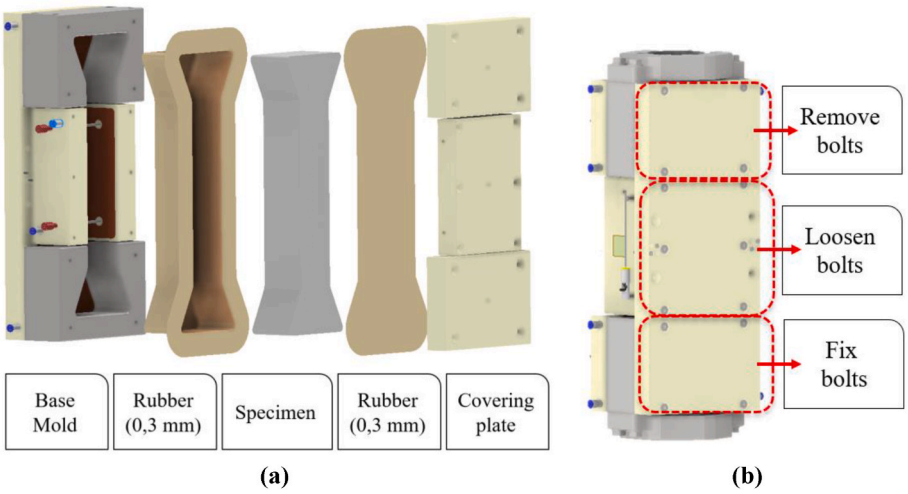

Fig. 5. Assembly of Mini-TSTM and ADTM: (a) Assembly steps; (b) Bolts removal.

installed to the universal loading machine. As shown in Fig. 5(b), the plugs were removed and the LVDTs should be set up for strain measurement as described in section 2.1.2. Moreover, at this step, the bolts connecting the plate CH1 to the plate B1 should be fully removed, to ensure that the upper cross head of the specimen can move freely. The bolts connecting the plates S1, S2 to the plate B1 should be loosened to remove lateral restraint to the specimen brought by plates S1 and S2. Only the four bolts connecting the plate CH2 to B1 should be fully fixed, which fulfills a fixed crosshead.

2.2. Improvements

In view of the concerns of existing TSTMs discussed in section 1.3, the Mini-TSTM results in the following improvements:

1) With the 3D printed plates, the mold of Mini-TSTM can be assembled and disassembled precisely and efficiently simply by bolting. The process of pre-test installation, casting, and post-test disassembling for the Mini-TSTM takes approximately 2 h for a single operator. For each Mini-TSTM and ADTM test, the volume of fresh material needed is around 0.7 L, which is significantly less than the existing TSTMs.
2) In the Mini-TSTM test, the full-restraint is achieved continuously by a PID controller. The PID controller takes the deformation measured by the LVDTs as input and continuously adjusts the applied force of the universal loading machine to fix the deformation at zero. Compared to the frequently used stepping control mode (see section 1.2), the Mini-TSTM does not require an input of threshold value which may influence the test result.
3) The strain in the Mini-TSTM is measured by only two LVDTs, less than most TSTMs introduced in section 1.2. The LVDTs are positioned at the middle (i.e., straight) part of the specimen and therefore the influence of stress concentration near the two crossheads can be eliminated. Meanwhile, The LVDTs are arranged at the two sides of the specimen and therefore any eccentric deformation of the specimen can be detected. The connection of LVDTs by magnetic blocks makes the assembly of LVDTs easier and more efficient compared to existing TSTMs.
4) In the Mini-TSTM test, the specimen is loaded vertically. Meanwhile, by removing the upper bolts and loosening the middle bolts, the specimen is detached from the covering plates. Therefore, in principle, the influence of friction that happens in most TSTMs (see section 1.2 is) eliminated in the Mini-TSTM test.

3. Methods and validation schemes

The validation of the Mini-TSTM and ADTM is conducted experimentally and theoretically. The experimental validation contains the tests for EAS evolution, elastic modulus, aging creep, and AD, which together form the experimental validation as shown in the left of Fig. 6. Afterward, the measured AD, elastic modulus, and aging creep compliance function will be used as input of a viscoelastic model to simulate the EAS evolution. Finally, the EAS evolution derived by the Mini-TSTM test, and the EAS evolution calculated by the viscoelastic model can be compared, as shown in the right of Fig. 6.

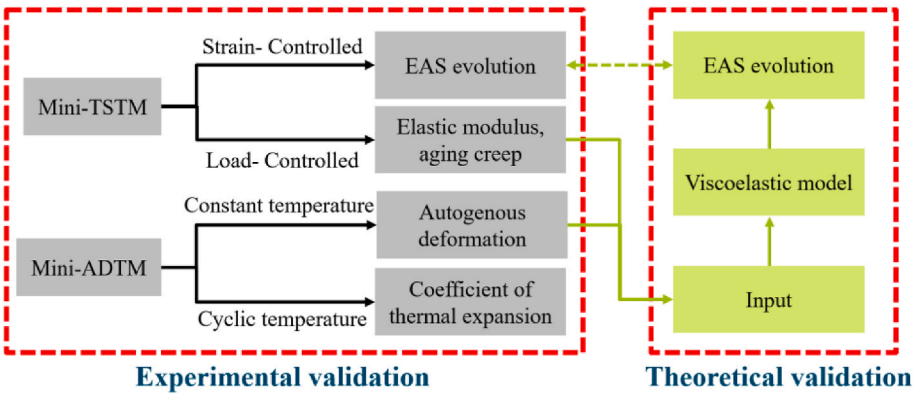

Fig. 6. Validation schemes.

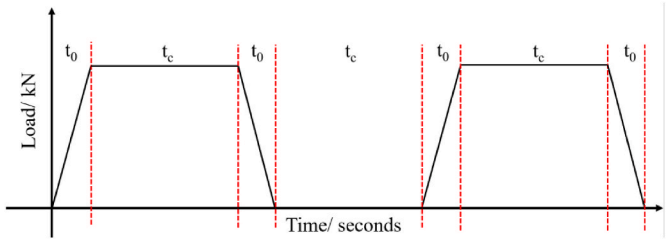

Fig. 7. Hourly repeated load for elastic modulus/aging creep test (t_0: 30 s loading time for testing elastic modulus; t_c: 3600 s sustaining at a constant load for testing creep).

3.1. Experimental methods

3.1.1. EAS test

The most common objective for TSTM is the EAS evolution, which is a direct index of EAC potential and therefore is the goal of all models related to EAC issues. To test the EAS evolution, the PID controller should be used to control the universal loading machine based on the input of LVDT, to fulfil the full-restraint condition as described in section 2.1.3. Besides, in this test, the temperature in the specimen is maintained constant (see section 2.1.3). Therefore, only the stress induced by AD is measured. The EAS evolution (measured by the Mini-TSTM) needs to be at the same time as the test of AD (measured by the Mini-ADTM). The same batch of fresh material should be used in these two tests. Of course, in real application the temperature will not be constant and the stress caused by restrained thermal expansion and contraction has to be included in the EAC. Furthermore, all properties, like autogenous shrinkage, E-modulus and creep will be influenced by the temperature changes. These influences are generally taken into account in FEM-models through a maturity concept model. The validity of these models will be studied with the setup at a later stage.

3.1.2. Elastic modulus and aging creep

The elastic modulus and aging creep are core parameters reflecting the viscoelastic properties of cementitious materials and directly determine how much stress can build up when the shrinkage is restrained. In this study, the elastic modulus and aging creep are key input parameters for the viscoelastic model to predict the EAS evolution, which can then be compared with the experimentally-measured EAS.

To test the elastic modulus and aging creep, an hourly-repeated load is applied to the sample. Assuming that the influence of aging within a time interval ranging from minutes to hours can be neglected, repeated load cycles were used to test the aging creep of cementitious materials at different ages [22,23]. In this study, the magnitude of the hourly-repeated load is determined by the TSTM test results, and the period of each cycle is 1 h. An example of the repeated load cycle for such a test is shown in Fig. 7. The hourly-repeated loading cycles consist of a loading phase, sustained load phase, unloading phase, and phase of sustaining at a nearly zero load. The loading and unloading phases are short (t_0 = 30 s in this study), allowing the elastic modulus at a certain age to be tested. Meanwhile, the loading speed ensures that the duration of the loading/unloading phase is smaller by two orders of magnitude compared to the creep test [23]. The sustained load phase at a certain load typically lasts longer (t_c = 3600 s in this study), allowing the creep compliance at a certain age to be tested. Aging creep needs to be tested at the same time as the test of AD test and using same batch of fresh material.

3.1.3. Autogenous deformation test

AD occurs due to cement hydration: self-desiccation effects induce internal capillary pressure and results in the contraction of the microstructure [24–28]. The thermal deformation and drying deformation are mainly the results of heat transport and moisture transport between the cementitious material and the environment and therefore depend on many factors including not only the material properties but also the structural geometry and environmental conditions [29–31]. In comparison, AD is an intrinsic material behaviour and the EAC issues it may induce are the main focus in the validation of the Mini-ADTM and Mini-TSTM. In the theoretical validation part, the measured AD will be used as input, together with the elastic modulus and aging creep, to predict the EAS results and compare with the EAS tested by Mini-TSTM.

To test the AD, the Mini-ADTM is used, which adopts the same type of mold as the Mini-TSTM, except that the plates CH1 and CH2 in Mini-TSTM are made of steel, while in Mini-ADTM they are made of 3D printing PA1200 powder. In this test, the Mini-ADTM just stands vertically and the temperature in the specimen is controlled at a constant value based on the temperature regulation system (see section 2.1.3). Therefore, thermal and drying deformation are excluded, and only the AD is measured.

3.1.4. Coefficient of thermal expansion (CTE) test

The test of CTE is performed to validate the following two aspects: 1) the reasonability of the measured evolution process of CTE; 2) the heating/cooling efficiency of the designed Mini-TSTM and ADTM systems, which will be shown by a fast heating/cooling temperature profile with a rate of 5 °C/hour; To test the CTE, the Mini-ADTM test is conducted under a cyclic temperature profile. An example of such temperature cycles is shown in Fig. 8(a). Under such temperature cycles, the total deformation measured by the ADTM is the sum of AD and thermal deformation. Assuming that within each temperature cycle, which lasts for $2t_T$, the effects of aging can be neglected and the AD is constant (i.e., $\varepsilon_{au,h} = \varepsilon_{au,c}$ in Fig. 8(b), where $\varepsilon_{au,h}$ and $\varepsilon_{au,c}$ stands for the AD during subsequent heating and cooling phase). Assuming that the coefficient of thermal contraction (CTC) is the same as the CTE [19], within the heating phase of each temperature cycle, the total deformation can be calculated as:

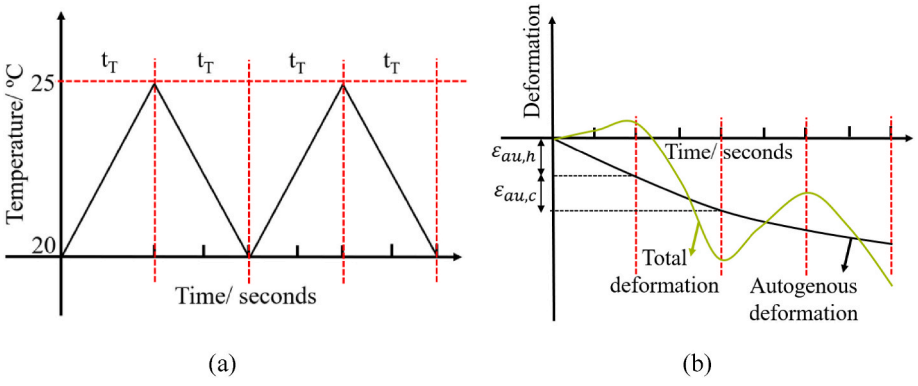

Fig. 8. Examples of a CTE test: (a) Temperature cycles; (b) Deformation.

Table 2
Main composition of utilized cements (wt.%).

Composition	CEM III/B	CEM I
CaO	47.11	64.00
SiO_2	29.11	20.00
Al_2O_3	10.02	5.00
MgO	5.89	–
SO_3	2.82	2.93
Fe_2O_3	1.19	3.00
Na_2O	0.28	0.58

Table 3
Detailed testing schemes for validation of Mini-TSTM.

Test	Material	Testing conditions	Objectives	Repetition
1	C1-30	LVDT- controlled full restraint Active/passive temperature control	EAS	C1-30-P1 C1-30-P2 C1-30-A1
2	C3-30	LVDT-controlled full restraint Active temperature control	EAS	C3-30-1 C3-30-2
3	C3-35	LVDT-controlled full restraint Active temperature control	EAS W/b influence	No
4	C3-30A	LVDT-controlled full restraint Active temperature control	EAS	No
5	C1-30	Load-controlled Active temperature control	Elastic modulus Aging creep	No
6	C3-30A	Load-controlled Active temperature control	Elastic modulus Aging creep	No
7	C3-30A	Free deformation Active cyclic temperature control	CTE Heating/ cooling	No

$$\varepsilon_{toh} = CTE \times \Delta T_h + \varepsilon_{au} \tag{1}$$

In the subsequent cooling phase, the total deformation can be calculated as:

$$\varepsilon_{toc} = CTC \times \Delta T_c + \varepsilon_{au} \tag{2}$$

where ε_{au} is the autogenous shrinkage in the heating/cooling phase; ΔT_h and ΔT_c are the temperature change in the heating and cooling phase, respectively; ε_{toh} and ε_{toc} are the total strains that happen in the heating and cooling phases, respectively. By calculating Eq (1) –Eq (2), one can calculate the CTE as follows:

$$\mathrm{CTE} = \frac{\varepsilon_{toh} - \varepsilon_{toc}}{\Delta T_h - \Delta T_c} \tag{3}$$

3.2. Detailed validation schemes

The validation of the Mini-TSTM is conducted by the tests described in section 3.1 based on cement paste made of two types of cement, CEM I 42.5N and CEM III/B 42.5N. Both cements were manufactured by the Eerste Nederlandse Cement Industrie (ENCI). The main chemical compositions of the two cements are listed in Table 2.

A detailed experimental validation scheme of the Mini-TSTM is listed in Table .3. The materials are labeled to show difference in cement types and w/b ratios. For example, "C1-30" stands for the material that uses CEM I and a w/b ratio of 0.30. In this study, it was found that even for the same type of cement, some testing results (i.e., initial shrinkage and autogenous expansion) can vary significantly if different batches of cement are used (see section 4). For the tests using CEM I paste, different batches of cement were used in different tests. For the cement type CEM III/B, two batches of cement were used. The C3-30 and C3-35 were from the first batch of CEM III/B, while the C3-30A was from the second batch. It should be stressed that this study aims to validate the proposed Mini-TSTM and Mini-ADTM setup. Therefore, while the variability of material behavior of the same type of cement can be detected by the proposed setup, the mechanisms behind this variability are outside of the scope of the current study.

In tests 1–6, both the Mini-ADTM and Mini-TSTM were performed at a constant temperature of 20 °C. In test 7, only the Mini-ADTM test was performed, and a cyclic temperature profile was used. In tests 1 and 2, the repeatability of the setup was examined. In test 1, both passive (C1-30-P1 and C1-30-P2) and active (C1-30-A1) temperature control methods were used. The active temperature control method has been described in section 2.1, where a PID controller will be used to actively adjust the water temperature to fix the temperature measured in the center of the specimen at a constant value (i.e., 20 °C). In comparison, the passive temperature control method is also used, which directly set the water temperature as the desired value (i.e., 20 °C).

3.3. Viscoelastic model

The stress buildup in a restrained cementitious material can be calculated by viscoelastic models, as shown in numerous studies [32–35]. In the Mini-TSTM test, the strain measurements are performed in the middle (i.e., straight) part of the dog-bone specimen, where stress should be evenly distributed because this part is far away from the cross-head (see section 2.1.2). Therefore, a 1-D model should be able to describe the stress buildup in the Mini-TSTM test. Considering cement paste as a viscoelastic material, the stress buildup in the Mini-TSTM test corresponds to a relaxation process, which can be calculated by the principle of Boltzmann superposition described as the convolution below:

$$\sigma(t) = \int_0^t R(t, t_0)\dot{\varepsilon}(t_0)dt_0 \tag{4}$$

where σ is the stress buildup calculated by the viscoelastic model; ε is the retrained strain; R is the relaxation modulus (GPa); t_0 is the time when deformation is restrained; t is the current time. By using the mid-point rule, the integration of Eq (4) can be simplified as:

$$\sigma(t) = \sum_{t_0=0}^{t_0=t} R\left(t + \frac{1}{2}\Delta t, t_0\right) \times \Delta\varepsilon(t_0) \times \Delta t_0 \tag{5}$$

The relaxation modulus can be derived from the creep compliance, which is easier to test. The creep compliance can be described by the double power law [36,37] as:

$$J(t, t_0) = \frac{1}{E(t_0)} + a * \left(\frac{1}{t_0}\right)^b * (t - t_0)^c \tag{6}$$

where a, b and c are fitting parameters that can be derived from tests, which reflect the impact of mix design, aging time and loading duration on creep evolution. Then, the relaxation modulus can be derived as follows [38–40]:

$$R(t, t_0) = e^{1 - J(t,t_0)E(t)}E(t) \tag{7}$$

In comparison, a 1D elastic model is also used, which can be described as below:

$$\sigma_{el}(t) = \int_0^t E(t)\dot{\varepsilon}(t_0)dt_0 \tag{8}$$

where σ_{el} is the stress buildup if the relaxation effect is neglected. Similarly, by the midpoint rule, Eq (8) can be simplified as:

$$\sigma_{el}(t) = \sum_0^t E\left(t + \frac{1}{2}\Delta t\right) \times \Delta\varepsilon(t) \times \Delta t \tag{9}$$

Based on the simple viscoelastic model in Eqs (4)–(7) or elastic model in Eqs (8) and (9), using the AD measured in tests 1–4, and the elastic modulus and aging creep measured in tests 5–6, the EAS can be

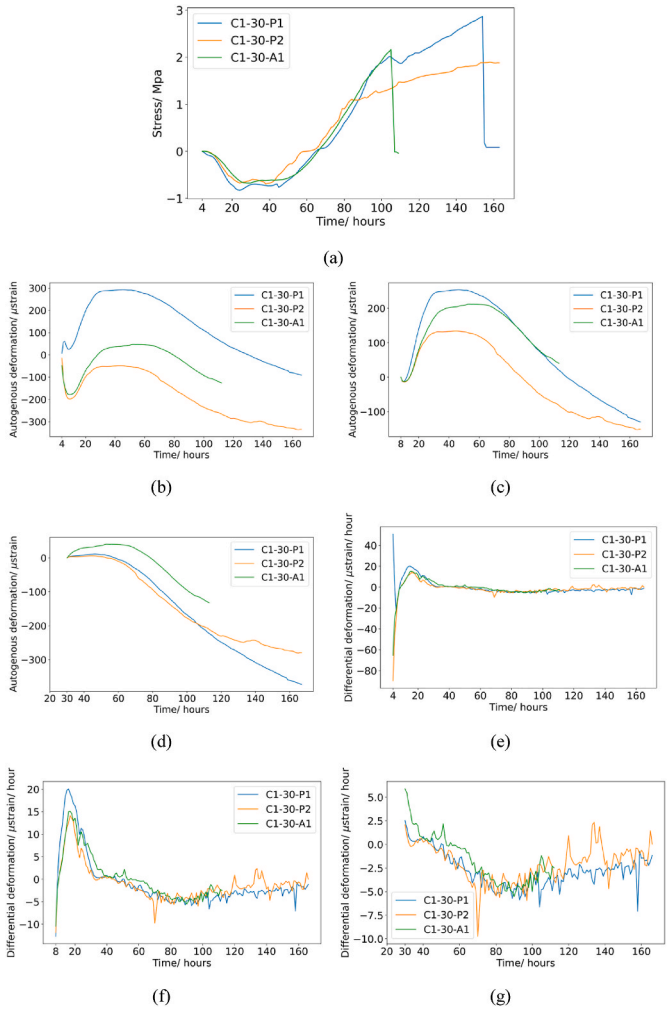

Fig. 9. EAS for CEM I paste with w/b = 0.30: (a) EAS; (b–d) AD zeroed at 4, 8, and 30 h; (e–g) First derivative of AD zeroed at 4, 8 and 30 h.

calculated and then compared with the EAS measured in tests 1–4.

4. Results and discussion

4.1. EAS test

By applying a full-restraint boundary condition, the EAS induced by AD can be tested, which is the most direct and important index for assessing early-age cracking potentials. In this test, to exclude the influence of thermal deformation, the temperature in the specimen is controlled at 20 °C. An analysis for examining the temperature control and strain control in the EAS tests is given in Appendix A.

4.1.1. EAS results of CEM I paste

The testing results of Mini-TSTM and ADTM for the CEM I paste with the w/b ratio 0.30 are shown in Fig. 9. In the three CEM I tests (C1-30-P1, C1-30-P2, and C1-30-A1), the batches of cement were different. The EAS (Fig. 9 (a)) and corresponding AD (Fig. 9 (b)) were recorded 4 h after the placement of fresh cement. AD is often characterized by a fast shrinkage in the first few hours followed by autogenous expansion and autogenous shrinkage, similar to the measurement of corrugated tube test [26]. For the three CEM I test, the AD was zeroed at the onset of autogenous expansion (i.e., 8 h as in Fig. 9 (c)) and the onset of autogenous shrinkage (i.e., 30 h as in Fig. 9 (d)). Based on the measured EAS (Fig. 9 (a)) and AD (Fig. 9(b–g)), the following mutual agreement between different tests validates the reasonability of the measurement:

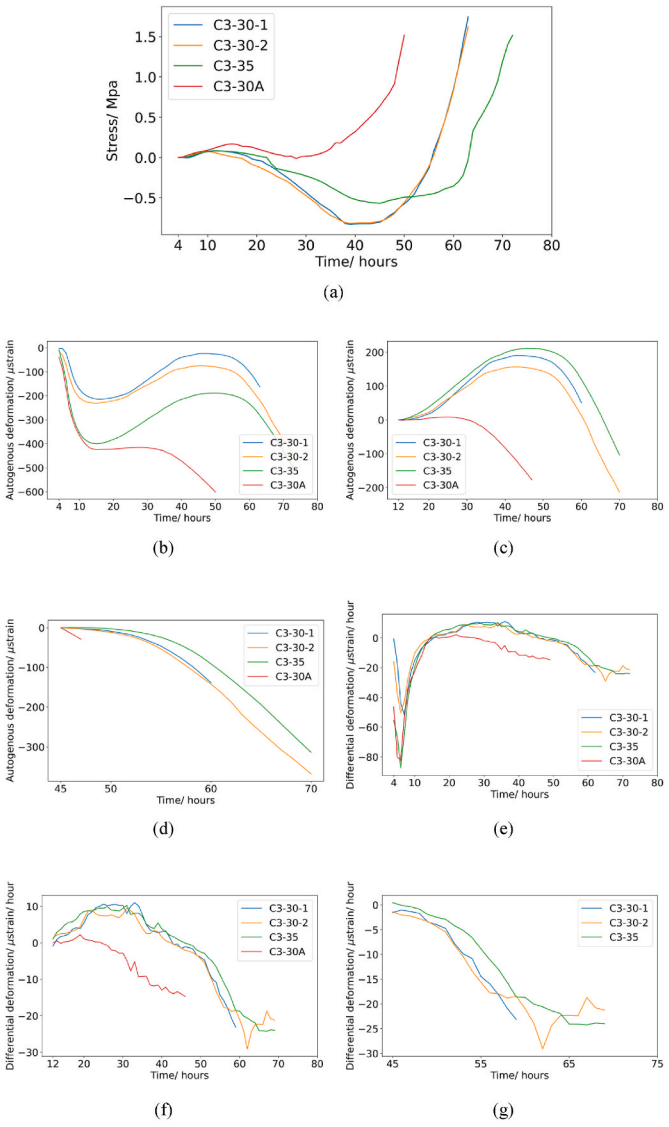

Fig. 10. EAS for CEM III/B paste with w/b = 0.30: (a) EAS; (b–d) AD zeroed at 4, 12, and 45 h; (e–g) First derivative of AD zeroed at 4, 12 and 45 h.

1) The expanding/shrinking process measured in the Mini-ADTM (Fig. 9(b–d)) corresponds to the stress decreasing (compression)/ increasing (tension) measured in the Mini-TSTM (Fig. 9 (a)).
2) The EAS of the three tests shows a similar trend and magnitude (Fig. 9 (a)). The C1-30-A1 cracked after around 100 h, while the C1-30-P1 cracked later, after 150 h. In the test for C1-30-P1, the loading machine of the Mini-TSTM stopped working at around 100 h, and therefore at that period, a drop of the load was observed, which stopped the specimen from cracking. The C1-30-P2 did not crack after 160 h.
3) The rate of AD of the three tests is similar (Fig. 9(e–g)). All tests for autogenous shrinkage after 30 h (Fig. 9 (d)) displayed good consistency and similar magnitude. Note that the rate of AD is a relevant than the absolute value since it directly determines the accumulation of stress (see Eq (4)).

Despite the consistency described above, significant variation in the absolute values of AD is found for the three tests, especially for the shrinkage at first 4–8 h (Fig. 9 (b)) and autogenous expansion at 8–30 h (Fig. 9 (c)). Note that due to batch difference of cement, the self-weight of the specimen and molds, and also slight difference in operations of the tests, high scatter in the measurement of the initial deformation can be

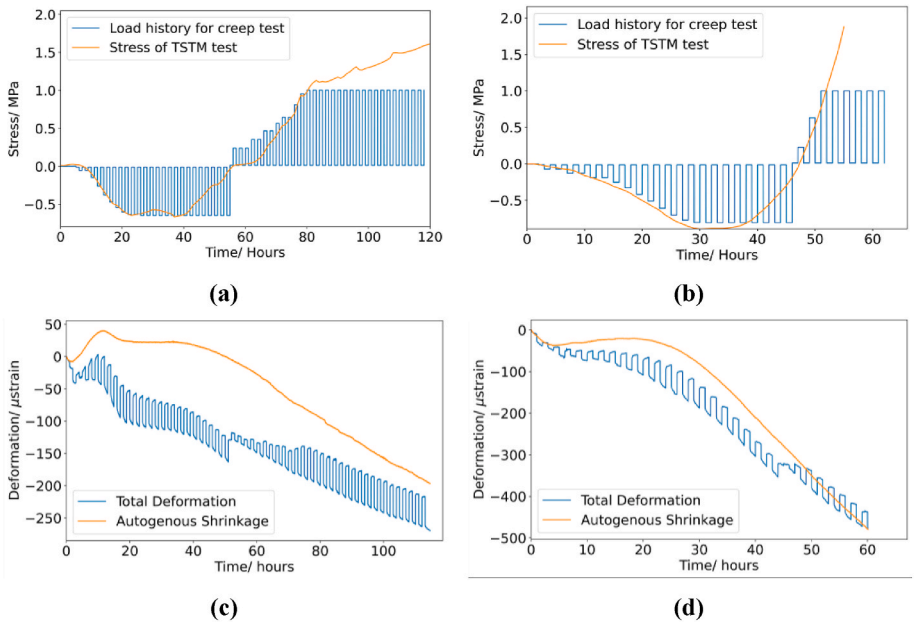

Fig. 11. Testing results for elastic modulus and creep of CEM I w/b = 0.30: (a–b) Hourly-repeated loading scheme for C1-30 and C3-30A, respectively; (c–d) Deformation results of the test for C1-30 and C3-30A, respectively.

induced, as pointed out by the systematic statistical study [41]. However, due to a very low elastic modulus and high creep/relaxation, a very high deformation only induces a very low stress and therefore such variation does not influence the EAS measurement, which has been quantitatively proved by the viscoelastic model in Appendix B. Specifically, according to the EAS result (Fig. 9 (a)), the measured stress at 4 h was 0.02, 0.04, and 0.03 MPa for the three tests C1-30-P1, C1-30-P2, and C1-30-A1, respectively. Therefore, the shrinkage at 4–8 h seems to be insignificant for the EAS buildup. Similarly, in the autogenous expansion phase at 8–30 h, the differences in compressive EAS (Fig. 9 (a)) are much less significant than that in the autogenous expansion (Fig. 9 (c)). This can also be explained by the low elastic modulus and high creep/relaxation of the cement paste in the first day.

In the authors' previous study [13], it was found that the autogenous expansion at 8–30 h is caused by the ettringite formation, which applies pressure on pore walls and leads to macroscopic expansion. In this process, the amount of ettringite determines the internal pressure, and the micromechanical properties (i.e., elastic modulus and creep) determine how much expansion can be obtained given a certain pressure [25,27]. Although significant difference in initial shrinkage and autogenous expansion is measured, the EAS results (Fig. 9 (a)) between the three tests remain similar. In section 4.4, solid quantitative explanations regarding why variation of early-age deformation does not influence EAS measurement will be presented by a verified viscoelastic model.

4.1.2. EAS result of CEM III/B paste

Development of EAS was tested in paste specimens with two w/b ratios (0.3 and 0.35) with CEM III/B. Meanwhile, two batches of cement were used, with the first batch of cement in tests C3-30-1, C3-30-2, and C3-35 and the second batch of cement in the test C3-30A. The tests C3-30-1 and C3-30-2 were for checking the repeatability of the Mini-ADTM and Mini-TSTM setup. The EAS results of the CEM III/B pastes are shown in Fig. 10. The EAS results on CEM III/B show the following consistency for validating the reasonability of the Mini-TSTM and Mini-ADTM setup:

1) In all four tests, the expanding/shrinking process as measured by the Mini-ADTM (Fig. 10(b)) corresponds well to the stress decreasing (compression)/increasing (tension) as measured by the Mini-TSTM (Fig. 10(a)).
2) For the two repetitive tests C3-30-1 and C3-30-2, excellent agreement in EAS results (Fig. 10(a)) and rate of AD (Fig. 10(e)) can be found.
3) In the expansion phase, the C3-30-1 shows a slightly higher expansion than C3-30-2. This is also reflected in the EAS result - a slightly higher compressive stress develops in C3-30-1. As also observed in the EAS results of CEM I (Fig. 10(a)), the difference in autogenous expansion is much more significant than that in EAS, which is caused by the low elastic modulus and high relaxation/creep which limit the compressive stress induced by this restrained expansion. This is explained in more detail quantitatively in section 4.4.
4) From (Fig. 10(b and c)), it can be seen that C3-35 shows higher expansion and lower shrinkage compared to C3-30. This difference is expected: with a higher w/b ratio, more ettringite will be produced, inducing higher expansion [13]. Meanwhile, a slower drop of relative humidity and larger pore sizes will occur in specimens with higher w/b ratio [26,27], resulting in lower internal capillary pressure (according to Kelvin's equation) and therefore eases the contraction that can be induced to the microstructure. As a result, the autogenous shrinkage for a higher w/b ratio should be lower (see Fig. 10(d)). However, it should also be noted that even with higher autogenous expansion, the compressive stress of C3-35 is lower than that of C3-30. This is attributed to the lower elastic modulus and higher relaxation/creep of a higher w/b ratio paste [42,43].
5) The consistent measurement of the AD and the EAS in the C3-30 and C3-30A tests shows that different batches of CEM III/B at the w/b ratio 0.30 can lead to completely different EAC potentials. Note that such complete difference in AD measurement was also observed and reconfirmed in the creep test and CTE test shown later. The difference between different batches of CEM III/B paste are analyzed as below:

i. The C3-30A shows higher initial shrinkage, almost no autogenous expansion, and much earlier and faster autogenous shrinkage afterward, as measured by the Mini-ADTM in (Fig. 10(b and c)). Accordingly, C3-30A obtained higher initial tensile stress in initial shrinkage phase (first 10 h in Fig. 10(b)), almost no compressive stress, and much earlier tensile stress accumulation in autogenous shrinkage phase commencing from around 24 h (Fig. 10(b)).

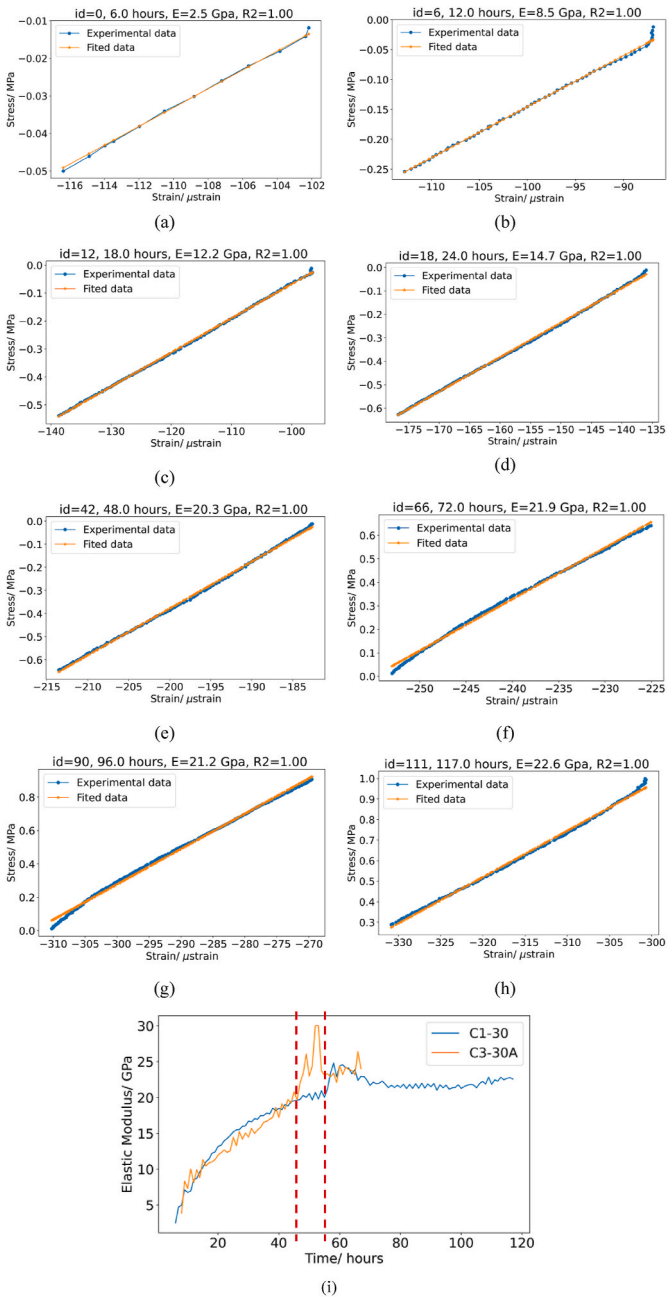

Fig. 12. Testing results for evolution of elastic modulus: (a–g) elastic modulus of C1-30 paste tested and calculated at 6, 12, 18, 24, 48, 72, 96, and 117 h; (i) summary of elastic modulus of C1-30 and C3-30A

ii. In comparison, the C3-30 tests showed very low initial tensile stress at first 20 h (Fig. 10(a)) and staying in compression in 20–52 h (Fig. 10(a)). Such significant difference clearly exposed the C3-30A to a higher risk of EAC and therefore the influence of batch difference of CEM III/B mix with a low w/b ratio on early-age AD should be an essential issue for cracking-sensitive structures.

6) The cracking time of C3-30A, C3-30, C3-35, and C1-30 is around 45, 58, 68, and 100 h, respectively. This is consistent with previous studies reporting that GGBFS concrete with a low w/b ratio shows higher risk of EAC due to autogenous shrinkage [13,44–46].

4.2. Measurement of elastic modulus and aging creep

Following the hourly-repeated loading method introduced in section 3.1.2, the time-dependent elastic modulus and creep of C1-30 and C3-30A paste were tested. In this test, the Mini-ADTM and Mini-TSTM were both used: Mini-ADTM to measure AD. and the Mini-TSTM to measure the elastic modulus and creep at different ages. The hourly-repeated loading scheme for C1-30 and C3-30A paste with a w/b ratio of 0.30 is shown in Fig. 11(a and b). To ensure that the applied load does not exceed the strength of the material and induce damage, the loading scheme was designed according to the EAS results of C1-30-P2 and C3-30-2 and the maximum tensile load was set to 2.5 kN. Accordingly, the AD tested by Mini-ADTM and the total deformation tested by Mini-TSTM is shown in Fig. 11(c and d). The test started at 10 and 14 h and lasted for around 117 and 60 h for C1-30 and C3-30A pastes, respectively. Note that the total deformation mentioned here includes the AD induced by hydration and basic creep strain induced by the sustained load.

To calculate the elastic modulus at different ages, the total deformation and stress at every loading and unloading period were extracted. Linear regression was used to calculate the elastic modulus at corresponding ages [47]. Examples of testing results and the calculation are given in Fig. 12(a–h). Finally, the evolution of elastic modulus of C1-30 and C3-30A along with time can be obtained, as shown in Fig. 12 (i). At around 46 and 55 h, the elastic modulus-time curve of C1-30 and C3-30A showed an upward jump and then decreased. The jump and the decreasing trend may be attributed to the transition from compression to tension and the sudden decrease in load level. Afterward, the load gradually increased from 0.75 kN to 2.5 kN (0.3 and 1 MPa in stress). Note that, when very low tensile load is applied (i.e., 0.3 MPa), the deformation may be small, resulting in a measurement error. With higher tensile load, the deformation will be larger, resulting in higher accuracy. However, the increasing tensile load may also induce internal damage to the specimen and therefore result in the decrease of elastic modulus. Note that to understand the influence of load (including level, compression/tension, loading/unloading) on the testing results of elastic modulus, a more refined testing scheme should be devised to exclude the influence of age, which is beyond the scope of the current study.

To calculate the creep at different ages, the total deformation measured by Mini-TSTM and the AD measured by Mini-ADTM at every hour were extracted. The basic creep compliance is calculated by deducting the AD from the total deformation and normalized by the corresponding sustained load level. As an example, the results of creep of C1-30 paste at different ages are shown in Fig. 13. To check the reasonability of the basic creep compliance results, all the basic creep curves were fitted to a non-aging power function ($J(t)=a\times t^{b}$) [36,47]. The quality of fitting was quantified by a coefficient of determination R^2 between the fitted and experimental values of creep compliance. A R^2 of 1 means a perfect fit is obtained and a R^2 lower than 0.70 were considered as incorrect testing data and removed. Finally, all the basic creep data were used to fit the double-power law function of aging creep (as expressed in Eq (6)). The results of fitting parameters are shown in Table 4. The obtained creep compliance function $J(t,t_0)$ is visualized in surface Fig. 13(i and j), which will be used for modelling the EAS based on input of shrinkage.

4.3. CTE test

Based on the methods introduced in section 3.1.4, the CTE of the C3-30A paste was measured, which aims to 1) provide a method for measuring CTE and 2) validate the temperature control ability of the proposed setup. The CTE test was performed on C3-30A using the Mini-ADTM, started 7.5 h and lasted for around 44 h. The results are shown in Fig. 14. Temperature cycles varying between 20 and 25 °C in every 2 h were adopted, as specified by the "Tmp_setpoint" curve in Fig. 14(a and b). The temperature results here also show the heating/cooling efficiency of the setup: To follow the specified temperature curves (i.e., "Tmp_setpoint" curve), at every turning point, the cryostat heated/cooled the water bath (i.e., "Bath" curve) to regulate the temperature of

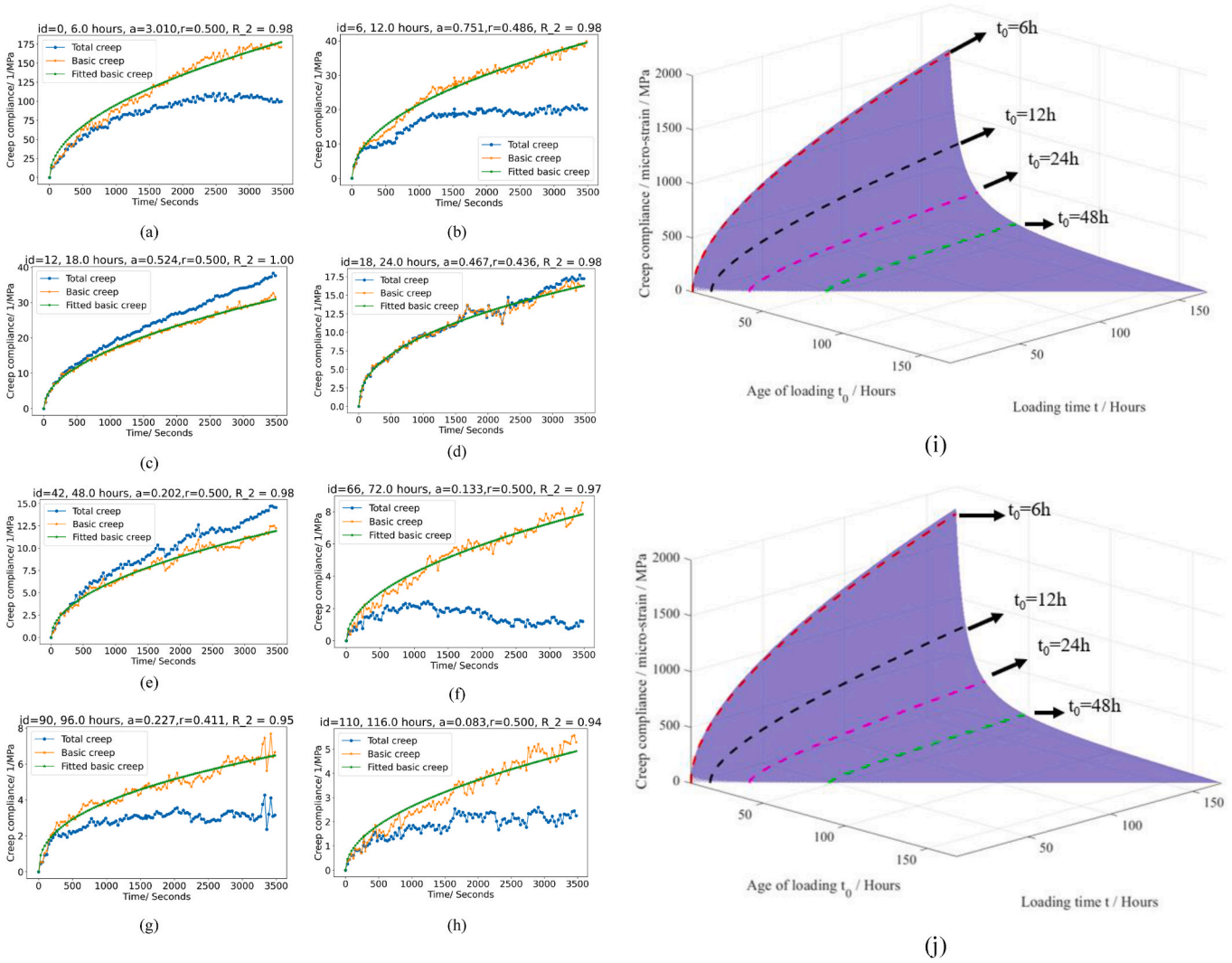

Fig. 13. Testing results for evolution of creep compliance: (a–g) creep compliance of C1-30 paste tested at 6, 12, 18, 24, 48, 72, 96 and 116 h; (i–j) summary of creep compliance of C1-30 and C3-30A.

Table 4
Fitting parameters obtained from creep test for creep compliance function.

Specimens	a	b	c	R^2
C1-30	1.000×10^5	1.079	0.500	0.8674
C3-30A	3.622×10^5	1.197	0.500	0.8655

the specimen (i.e., "Tmp" curve) based on the PID controller, as mentioned in section 2.1.3. As clearly shown in Fig. 14 (b), when reaching the turning point, it took about 10 min for the cryostat to adjust the temperature of the water bath to adapt to the new heating/cooling curve, and therefore there was always an overshooting observed in the specimen temperature. Afterward, the specimen temperature can be precisely regulated to follow the specified temperature curve. With the temperature cycles, the total deformation is a superposition of continuous AD and cyclic thermal deformation, as shown in Fig. 14 (c). Assuming that within every 2 h the rate of AD stays the same, the influence of AD can be eliminated by taking the average of deformation measured in the heating and cooling phase, as shown in Fig. 14 (d) and explained by Eqs (1)–(3). The CTE of each temperature cycle was calculated using linear regression [47] and the evolution of CTE is shown in Fig. 14 (e). An increase in CET was observed from around 6.6 to 14.4 μstrain/°C on the first and second day, which is in accordance with the literature [17,18].

4.4. Modelling results

Based on the AD measured from 4 h after casting (section 4.1), the elastic modulus, and the aging creep (section 4.2), the EAS can be predicted using the viscoelastic models proposed in section 3.3. The result can then be compared to the EAS measurements (section 4.1) to check if all the measured subjects match each other based on the viscoelastic constitutive relationship. Specifically, the ADs measured from 4 h after casting in tests C1-30-P1, C1-30-P2, C1-30-A1, C3-30-1, C3-30-2, and C3-30A were used as input to calculate the EAS in corresponding tests. For the input of elastic modulus and aging creep, the test performed on C1-30 and C3-30A were used for CEM I (i.e., C1-30-P1, C1-30-P2, C1-30-A1) and CEM III/B (i.e., C3-30-1, C3-30-2, and C3-30A) paste, respectively. The modeling results of EAS and comparison to the experimental results are shown in Fig. 15. The root mean square error (RMSE) between the modeling and experimental results of EAS were calculated to show the precision obtained by the models:

$$RMSE = \sqrt{\frac{\sum_t (\sigma_M(t) - \sigma_T(t))^2}{t_{total}}} \tag{10}$$

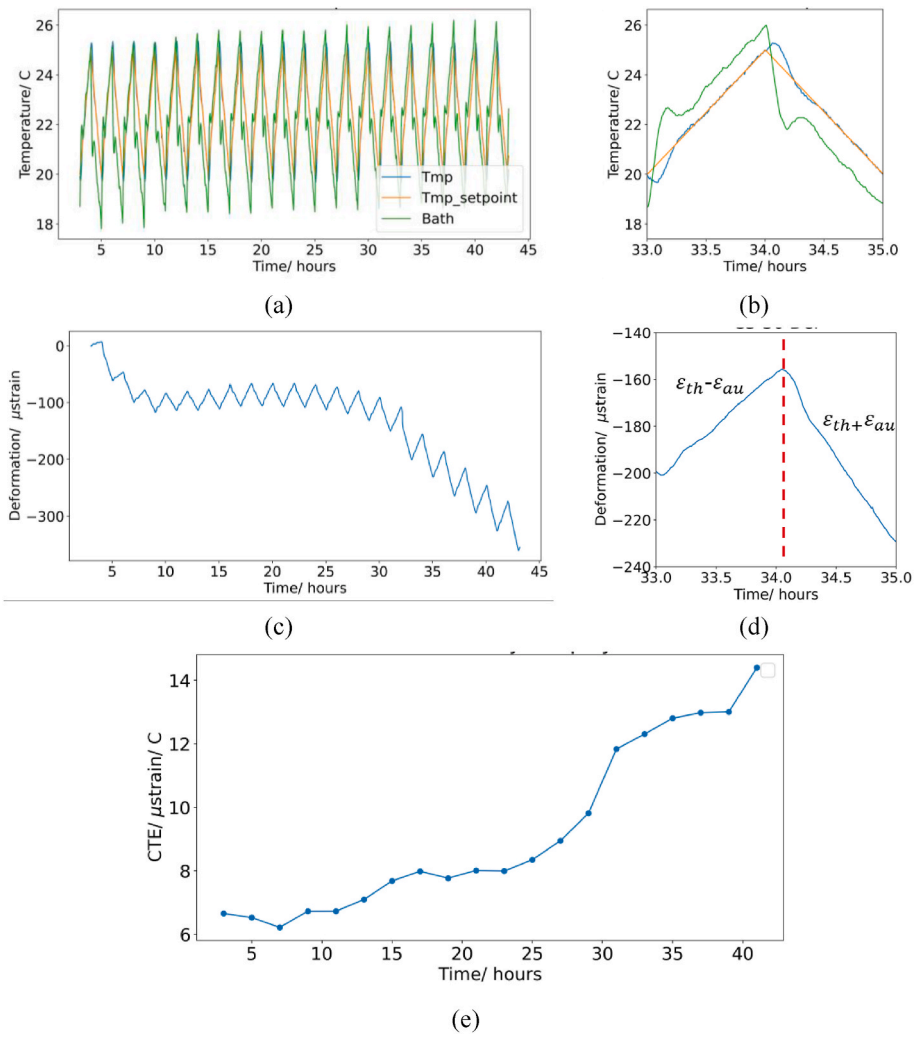

Fig. 14. Testing results for evolution of CTE of C3-30A paste: (a–b) temperature history; (c–d) total deformation; (e) CTE.

where $\sigma_M(t)$ and $\sigma_T(t)$ are modelling and testing results of EAS at time step t. The results in Fig. 15 show a good match between the EAS calculated by the viscoelastic model and the results directly obtained from the EAS test. As expected, the influence of creep/relaxation must be considered in EAS calculation and therefore an elastic model is not acceptable for the prediction of EAS. It should be noted that in most cases neglecting viscoelastic behavior will be conservative and result in a lower risk for early age cracking, but in other cases the opposite will happen and the risk for early age cracking will increase.

Despite the significant differences in the measured initial shrinkage and autogenous expansion of C1-30-1, C1-30-2, and C1-30-3 (presumably caused by using different cement batches), the calculated EAS results for these three tests are similar to the testing results. In the CEM III/B tests, although with a completely different AD and EAS between the batch 1 (i.e., C3-30-1 and C3-30-2) and batch 2 (i.e., C3-30A), their EAS can still be predicted with good accuracy given the corresponding AD as input. What is more interesting is that only using the elastic modulus and creep tested on C3-30A as input, the EAS results of C3-30-1 and C3-30-2, which are of different batches of cement and show totally different AD, can still be predicted with good accuracy. Such good accuracy means that the batch difference of CEM III/B does not result in a significant difference in mechanical properties (i.e., elastic modulus and creep in this case). In conclusion, the good match between the modeling and the experimental results directly validates that the devised Mini-TSTM and ADTM setup can detect the true material behavior and properties with good accuracy.

4.5. Discussion on potential limitations and improvement

This paper develops a Mini-TSTM, which aims to improve the efficiency of TSTM-type test for a range of properties/behaviors of early-age cementitious materials. The applicability of the designed Mini-TSTM has been validated by a systematic study of experiments and models. Herein, the limitations, major concerns and potential improvement are summarized and discussed as below:

1) In the Mini-TSTM test, a dog-bone specimen with a size of 50 × 50 mm^2 is used, which raises the concern about its applicability on concrete mixture where large aggregates should be used. To this regard, additional tests on concrete materials were conducted, see Appendix C. The Mini-TSTM was applied to test the EAS and total deformation of a concrete mixture that is specifically designed for underground concrete structure constructions. In the meantime, the same batch of concrete material was also used to do a traditional TSTM test at the TU Delft. In general, the results show a good consistency between Mini-TSTM and traditional TSTM, and therefore the applicability of the current Mini-TSTM setup for concrete materials with aggregate size up to 22 mm is validated. Nevertheless, it should be noted that the specific section size depends on multiple factors including the loading capacity, maximum aggregate size, expected stress range, etc., and is always adjustable accordingly.
2) Another concern about the Mini-TSTM is the vertical loading, which differs with most traditional TSTMs. Such change brings advantages,

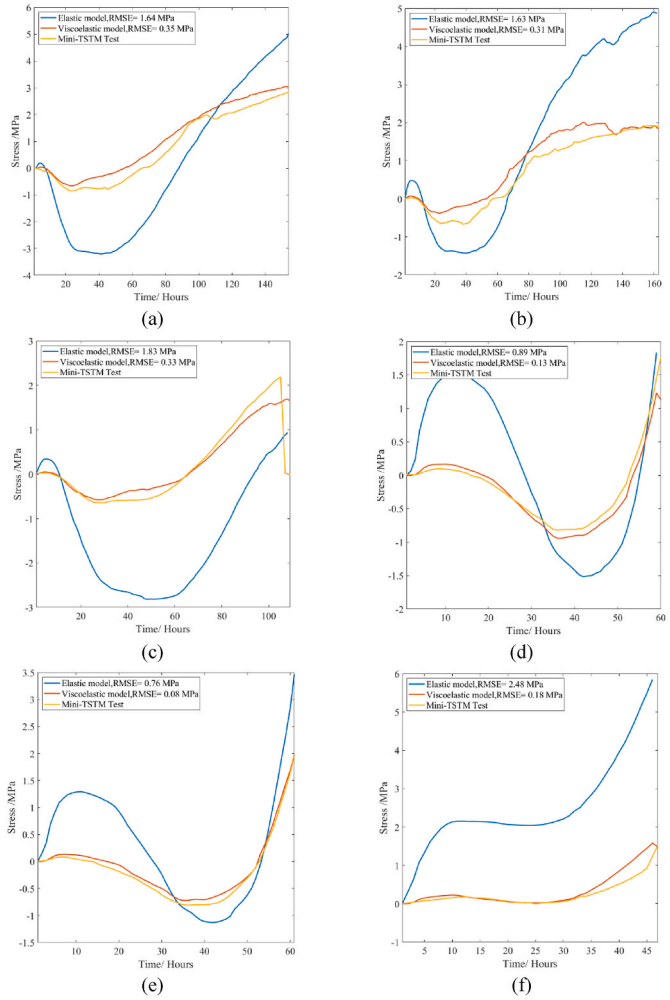

Fig. 15. Modelling results and comparison to EAS test: (a–c) results of CEM I paste C1-30-1, C1-30-2 and C1-30-3, respectively; (d–f) results of CEM III/B paste C3-30-1, C3-30-2, and C3-30A, respectively.

that the potential influence of the friction between the supporting plate and the TSTM specimen is eliminated. However, the self-weight of the specimen can influence the deformation measurement in the vertical test. For very young and soft specimen, the self-weight of the specimen and the molds causes “settlement deformation” and the measurement of shrinkage in very early-age in the vertical test can therefore be overestimated. However, as explained in Appendix B, due to the low elastic modulus and high relaxation at very early-age, such deformation can only lead to negligible stress, and therefore does not influence the EAS measurement.

3) In each testing batch, even a slight difference in material compositions, quantity, vertical position alignment, and bolts assembly, can influence the testing results, especially the deformation at very early-age. The reason is similar to that of the vertical-loading test. For a very young and soft specimen, a slight difference in self-weight or mechanical alignment can cause apparent difference in the very early-age deformation. However, as stated before and also explained in Appendix B, the deformation during this period does not significantly influence the EAS evolution and therefore the EAS results are repeatable. It should be noted that this limitation is not specifically for the Mini-TSTM. For the traditional TSTM, in which the testing procedures are far more complex and more difficult to control, such influence can be more significant.
4) The designed Mini-TSTM uses a dog-bone specimen and measures the middle straight area with a length of 100 mm, which requires a more sensitive LVDT when concrete with very slow shrinking rate is used. The inadequacy of precision of LVDT is one reason accounting for the unsmooth curves as observed in Mini-TSTM tests for concrete in Appendix C. Therefore, if the EAC issue of concrete is the main interest, it is suggested to lengthen the area of measurement or use a more sensitive LVDT.

5. Conclusions

This article describes the development of a light and small version of Mini-TSTM and Mini-ADTM. The developed setups allow more efficient measurement of time-dependent behaviors and properties of cementitious materials related to EAC issues, including the EAS, autogenous/thermal deformation, elastic modulus, creep and CTE. The design, implementation and methods of the new setup and experiments are introduced in detail. A systematic validation scheme, from the perspective of experiments and theories, was conducted to examine the reasonability of the proposed setup. The study resulted in the following conclusions:

1) The Mini-ADTM and Mini-TSTM, made mainly by 3D printing techniques, improved the testing efficiency and addressed several issues in big TSTM and ADTM tests, including the difficulty in pre-test installation and post-test dissembling, continuous control for full-restraint condition, LVDT installation, and friction between the specimen and supporting table.
2) The Mini-ADTM and Mini-TSTM showed good consistency in EAS test. The expanding/shrinking process detected by the Mini-ADTM matched well with the stress decreasing (compression)/increasing (tension) detected by the Mini-TSTM. The influence of cement type and w/b ratios on EAC potentials were correctly reflected. The heating/cooling efficiency of the proposed setup was examined in a CTE test, which obtained reasonable results compared with existing studies.
3) The Mini-ADTM and Mini-TSTM showed good repeatability. In EAS tests of CEM I, all mixes obtained similar EAS despite a significant difference was found in measurement of early shrinkage and autogenous expansion. In EAS tests of CEM III/B, the results from the same batch C3-30-1 and C3-30-2 also showed good repeatability in measurement of both AD and EAS. In EAS tests of concrete with aggregate size up to 22 mm, the EAS and total deformation measured by Mini-TSTM/ADTM and traditional TSTM/ADTM resembles each other and validated the applicability of the Mini-TSTM for concrete.
4) The Mini-ADTM and Mini-TSTM found that batch difference of CEM III/B mix with a low w/b ratio (0.30 in this study) can result in a completely different EAC potential. The C3-30A batch showed a faster initial shrinkage, almost no autogenous expansion and earlier autogenous shrinkage, which led to higher EAC risk.
5) The measured AD, elastic modulus and creep can be used as the input of a viscoelastic model to predict the EAS with good accuracy, which validated that the proposed setup correctly simulated and measured the process of EAS evolution. By comparing the results of viscoelastic model and elastic model, it is found that in some cases neglecting viscoelastic behavior will be conservative and result in a lower risk for EAC, but in other cases the opposite will happen and the risk for EAC will increase. Simulating the EAS evolution of one batch of CEM III/B (i.e., C3-30-1 and C3-30-2) based on the elastic modulus and creep data measured on another batch of CEM III/B (i.e., C3-30A) shows good accuracy. The same holds for CEMI-mixes.
6) It was shown quantitatively (i.e., using the viscoelastic model) that the lower elastic modulus and high relaxation are the reasons that the initial shrinkage and autogenous expansion at an early age played a much less significant role on stress development than autogenous shrinkage afterward.

CRediT authorship contribution statement

Minfei Liang: Conceptualization, Data curation, Investigation, Methodology, Validation, Writing – original draft. **Ze Chang:** Investigation, Validation, Writing – review & editing. **Patrick Holthuizen:** Formal analysis, Writing – review & editing. **Yu Chen:** Formal analysis, Writing – review & editing. **Shan He:** Investigation, Writing – review & editing. **Erik Schlangen:** Conceptualization, Methodology, Supervision, Writing – review & editing. **Branko Šavija:** Formal analysis, Methodology, Supervision, Writing – review & editing.

Declaration of competing interest

The authors declare that they have no known competing financial interests or personal relationships that could have appeared to influence the work reported in this paper.

Data availability

Data will be made available on request.

Acknowledgements

Minfei Liang would like to acknowledge the funding supported by China Scholarship Council under grant number 202007000027. Branko Šavija acknowledges the financial support of the European Research Council (ERC) within the framework of the ERC Starting Grant Project "Auxetic Cementitious Composites by 3D printing (ACC-3D)", Grant Agreement Number 101041342.

Appendix A. Analysis of temperature and strain control in EAS tests

In the EAS test for CEM I, two temperature control methods were used: passive control (C1-30-P1 and C1-30-P2) and active control (C1-30-A1). C1-30-P1 and C1-30-P2 are two repetitive tests with the same w/b ratio. As shown in Fig. A1, taking the C1-30-P1 as an example, passive control (see Fig. A1 (a)) works by keeping the temperature of the water at the target value (20 °C); on the other hand, active control (see Fig. A1 (b)) takes feedback from the measurement of thermocouples embedded in the specimens and actively adjusts the water temperature to enforce the temperature measured by thermocouples (embedded in the specimen) at a fixed value (20 °C). The temperature results show that active control method can perfectly keep the temperature of the specimen at 20 °C (blue line in Fig. A1 (b)) by more cooling within the first day (orange line in Fig. A1 (b)) to compensate for the hydration heat and room temperature. In comparison, the passive control shows only a limited effect: the temperature in the specimen increased to 21.5 °C due to hydration heat release, and then slowly decreased to 20.5 °C. Overall, to strictly exclude the influence of temperature and ensure that only the AD is considered, active control method is preferred.

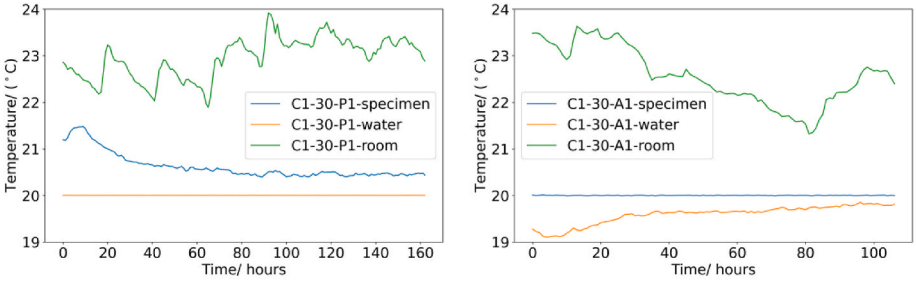

Fig. A1. Temperature measurement in EAS test for CEM I paste: (a) Passive control; (b) Active control

As shown in Fig. A2, with the PID controller which takes the strain measured by the LVDTs as feedback to continuously adjust the applied load, the deformation in the specimen in the Mini-TSTM can be controlled within 1 μstrain (0.1 μm). In other words, the full-restraint condition in the Mini-TSTM is achieved with a precision of 1 μstrain.

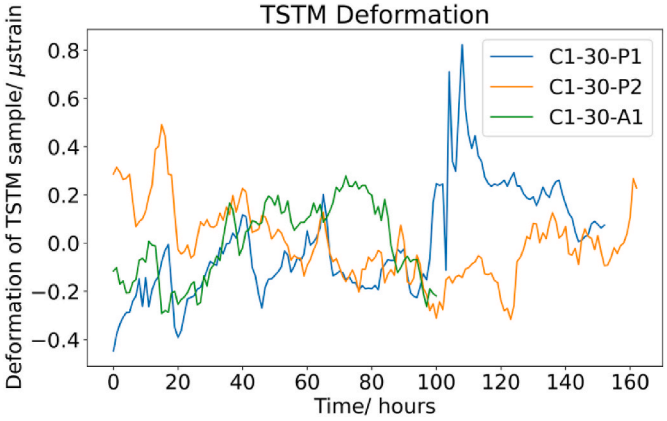

Fig. A2. TSTM deformation under full-restraint condition

Appendix B. Variation analysis of autogenous deformation

To explain why such a significant variation in early chemical shrinkage and autogenous expansion causes only a small difference in EAS, detailed quantitative explanations are given from two aspects: 1) a sensitivity study and 2) the principle of stress superposition.

Sensitivity study

Taking the EAS and AD of C1-30 as an example, one can see that the AD can be divided in 4 stages:

1) S1: fast shrinkage in 1~10 h;
2) S2: fast expansion in 10~20 h;
3) S3: small deformation in 20~50 h;
4) S4: fast shrinkage after 50 h.

To show the influence of variation of AD on the EAS, a sensitivity study is conducted based on the viscoelastic model. The sensitivity study assumes that a fictitious AD of 100 μstrain happens linearly from t_0 and lasts for 10 h. Accordingly, using the measured creep function of C1-30 as input, the EAS of the period corresponding to the fictitious AD can be calculated. Four different scaling factors (i.e., 0.5, 1.0, 1.5, 2.0) are used to scale the magnitude of AD and compare the variance of calculated EAS. The example of the fictitious AD and corresponding EAS happening from 1 to 41 h ($t_0 = 1, 41$) are shown in Fig.B1. By calculating the variance of the EAS induced by AD of different magnitudes at different t_0, the influence of AD on the EAS evolution can be quantified. From 1 to 100 h, the variance of EAS in each 10-h interval can be calculated, as shown in Fig.B2. The results show that the variant AD happening in Stages 1 and 2 (i.e., S1 and S2 in Fig.B1) can only result in negligible variance of EAS, which explains why the variation of initial shrinkage and expansion does not make an apparent difference in the EAS.

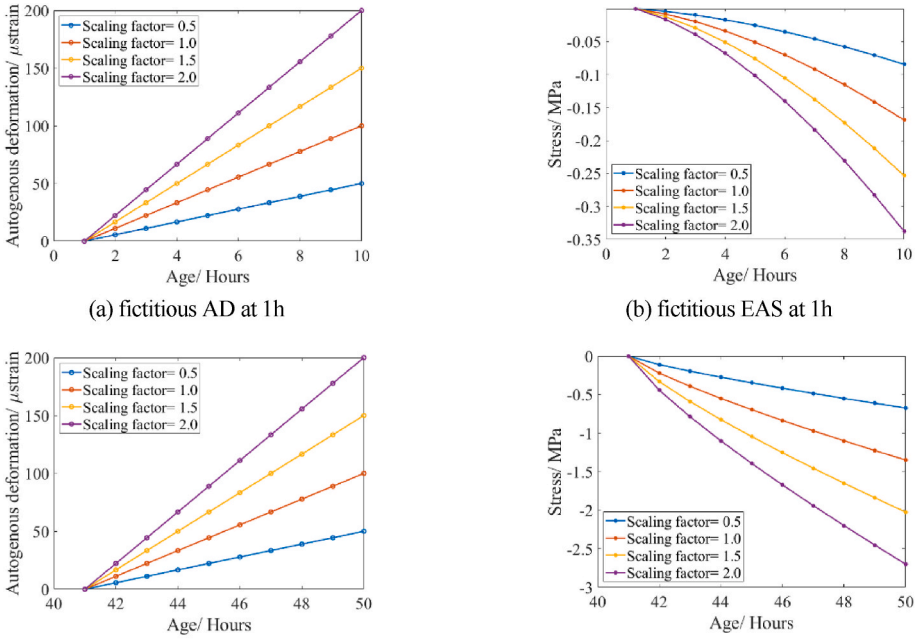

Fig. B1. Examples of sensitivity study: (a, c) fictitious AD happening at $t_0 = 1$ and 41 h; (b, d) Fictitious EAS caused by the fictitious AD.

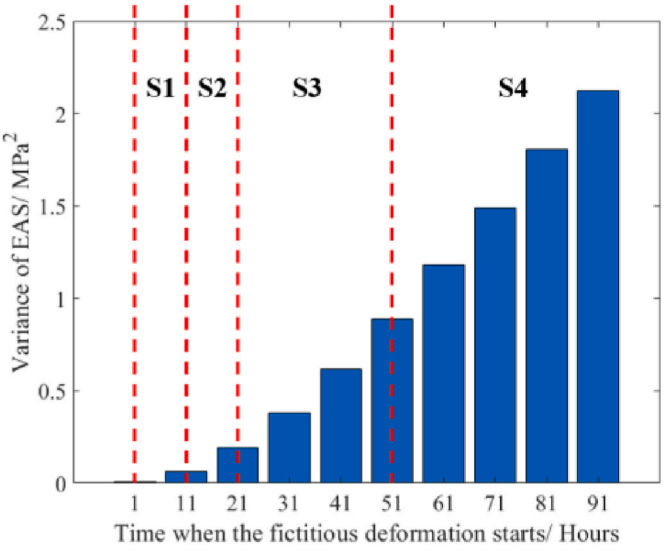

Fig. B2. Variance of EAS induced by fictitious AD (S1: fast shrinkage in 1∼10 h; S2: fast expansion in 10∼20 h; S3: small deformation in 20∼50 h; S4: fast shrinkage after 50 h)

Stress superposition

The viscoelastic model is built based on the Boltzmann superposition principle, which assumes that the stress at a certain time is a superposition of all the stress increments of all previous time intervals. Using the modelling case of C3-30-1 as an example, the stress increment at every time interval is shown in Fig.B3. Fig.B3 (a) shows that in every time interval, the stress instantly increases, which is an elastic response to the restrained shrinkage in the corresponding time interval (i.e., autogenous shrinkage rate as in Eq (5)). The magnitude of the instant stress increase depends on both the autogenous shrinkage rate and the elastic modulus of the material. Furthermore, the stress starts to decrease with time due to the viscous nature (i.e., creep/relaxation) of the material and is quantified by the relaxation modulus $R(t, t_0)$, which is calculated based on the creep compliance surface function $J(t, t_0)$ as measured by the Mini-ADTM and Mini-TSTM. Fig.B3 (b) shows the stress at incremental time steps 4, 30, and 55 h, which corresponds to the initial shrinkage, autogenous expansion, and autogenous shrinkage phase. Due to relaxation and creep, the stress increment starting from 4 h (within the initial chemical shrinkage phase) almost disappears after one day and that starting from 30 h (within the autogenous expansion phase) significantly decreases (by 70 %) at 60 h. The stress increment starting from 55 h only decreases by 20 % at 60 h. Note that the EAS test of C3-30-1 only lasts for 60 h. If considering later times, such as 168 h, one can find in Fig.B3 (a) that the stress increment starting from phases of chemical shrinkage and autogenous expansion both almost disappear, and only that starting from the phase of autogenous shrinkage remains at a certain level.

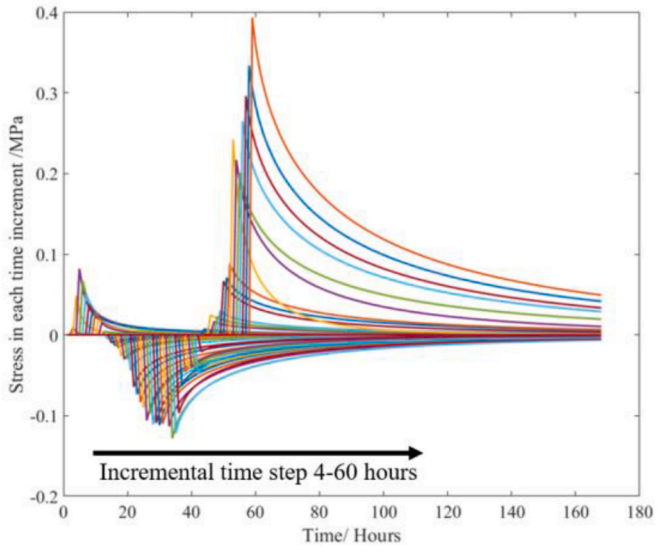

(a)

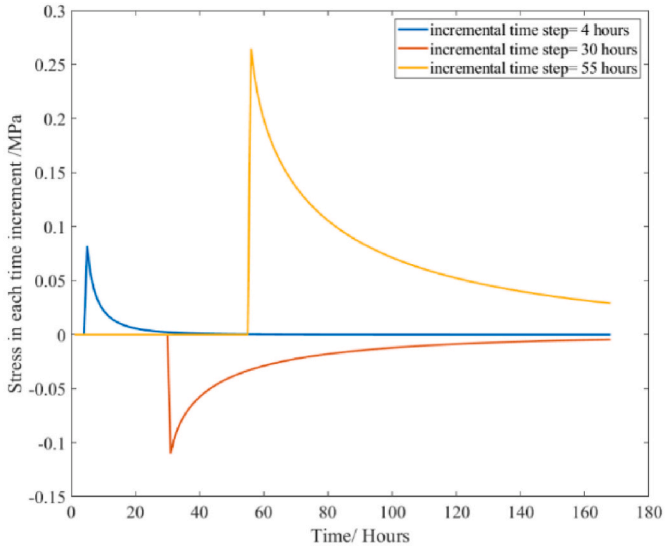

(b)

Fig. B3. Stress increment of C3-30-1 modelling result: (a) stress increment at every hour; (b) stress increment at 4, 30, and 55 h

Appendix C. Mini-TSTM for Concrete and Comparison to Traditional TSTM

Considering the size of the Mini-TSTM, notable potential limitations are about its applicability for concrete and its difference with the traditional TSTM. To this regard, we present additional results of EAS tests on a normal concrete mixture using both the developed Mini-TSTM and the traditional TSTM at the TU Delft, as shown in Fig. 3 [13]. The details of the concrete mixture are shown in Table C1. The concrete mixture used here is specifically applied in large-scale underground constructions, where early-age cracking risk is a governing factor in the design process. The utilized binder is Portland-Fly Ash cement CEM II/A-V 42.5N. The aggregates were all obtained from the Norsk Stein Jelsa. The admixture includes air entraining (AE) MasterAir 22SB, superplasticizer MasterGlenium SKY 851 (labeled as SP1 below), and MasterPozzolith 120 (labeled as SP2 below).

Table. C1
Concrete mixture for TSTM tests (Unit: kg/ m^3)

CEM II/A-V	Aggregate 0–2 mm	Aggregate 2–8 mm	Aggregate 8–16 mm	Aggregate 16–22 mm	Water	AE	SP1	SP2
410	697.25	214.67	613.5	321.92	120.92	1.108	3.280	1.435

The compressive and tensile splitting strength is tested at 1, 3, and 7 days. Each test uses three 150 × 150 × 150 mm^3 cubic specimen and the averaged results are shown in Table. C2.

Table. C2
Strength test results (Unit: MPa)

Age (day)	Compressive strength	Tensile Splitting strength
1	17.6	1.68
3	34.9	3.60
7	48.8	4.70

In this TSTM test, instead of testing the EAS at a constant temperature (as what have done in this paper), a time-dependent temperature profile is applied to simulate the in-situ temperature increase and decrease in concrete structures. The applied temperature curve is shown in Fig. C1. The temperature increases from around 23.5 °C–37.5 °C in the first day, and then decreases afterward. Notably, Fig. C1 shows a discontinuity at around 25 h between the two TSTMs. Such inconsistency is attributed to a malfunction of the cryostat, which stopped the temperature control for around 1 h. Afterward the temperature control was restarted, which ensured that the temperature curves in two TSTMs assemble each other.

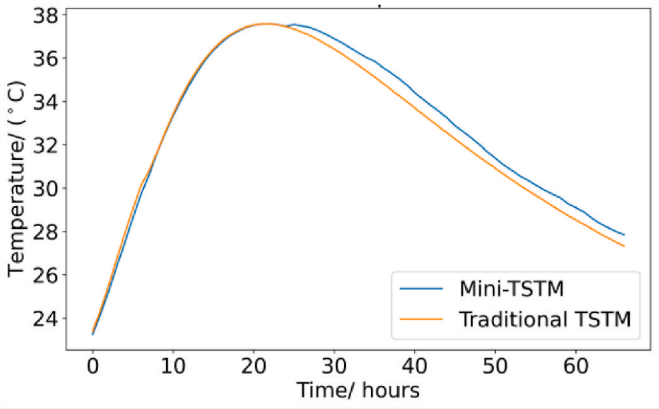

Fig. C1. Applied temperature curve in Mini-TSTM and TSTM test

Following the procedures of traditional TSTM, both TSTM tests were started around 12 h after casting, and then lasted for around 3 days. The obtained results of EAS and deformation by the Mini-TSTM and traditional TSTM tests are shown in Fig. C2 below. The results show a good consistency between the Mini-TSTM and the traditional TSTM, which further validates the applicability of the Mini-TSTM for concrete materials. Note that the same batch of mixture material were used here for both tests, and therefore the batch difference as appeared in the paper does not exist here, which is beneficial for direct comparison of the two tests. Nevertheless, despite the good consistency, some notable difference exists, explained as below:

1) The shrinking rate of the Mini-ADTM is faster than that of traditional ADTM. Accordingly, the EAS increase rate of the Mini-TSTM is also faster. This difference can be attributed to the vertical testing of the Mini-TSTM, in which the gravity also plays a role and the self-weight of the specimen (and also the molds) can lead to more vertical settlement of the specimen, which appears as more "shrinkage" in the final measurement. This effect is especially apparent when the specimen is very young (e.g., before first three days), when the elastic modulus is low so that only the self-weight can induce non-negligible deformation. However, as explained in Appendix B, during this period, because of very high relaxation effects, such deformation can only induce very low-level stress. Because the TSTM mainly aims to measure the EAS as the direct index of EAC risk, the side effects of vertical loading do not influence the main function of the testing machine.
2) Another notable difference is that the results of Mini-TSTM seems to be much less smooth. This is attributed to the inadequate precision of the current LVDTs for this test. In the Mini-TSTM test for concrete, the shrinking rate of the concrete specimen is less than 2 μstrain/hour (i.e., 0.2 μm/hour), while the precision of the utilized LVDT in Mini-TSTM is 0.01 μm. Considering that every second the loading machine needs to adjust the load to restrain the deformation, the inadequate precision of LVDT can bring noise to the machine and therefore causes jumps in the EAS results. A good example of such is the Mini-TSTM results of the C3 cement paste as shown in section 4.1.2, where much more smooth curves can be obtained when the shrinking rate is high. To address this issue, further improvement of the Mini-TSTM setup can consider to use either better LVDTs or simply by increasing the measurement area of the dog-bone specimen.

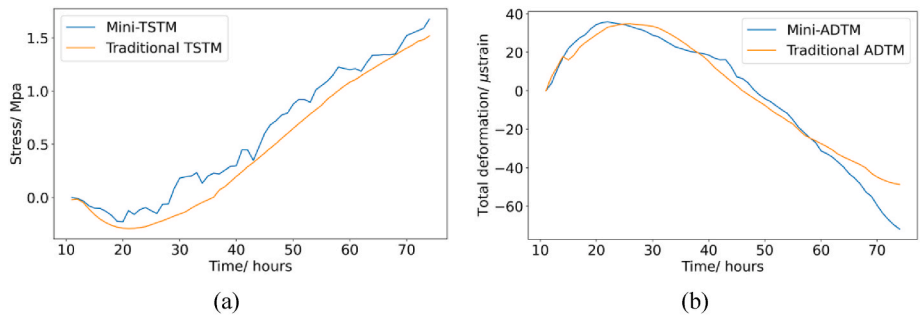

Fig. C2. Applied temperature curve in Mini-TSTM and TSTM test: (a) EAS; (b) Total deformation.

References

[1] R. Spingenschmid, Prevention of Thermal Cracking in Concrete at Early Ages, E&FN Spon, London, 1998.

[2] M. Briffaut, F. Benboudjema, L. D'Aloia, Effect of fibres on early age cracking of concrete tunnel lining. Part I: laboratory ring test, Tunn. Undergr. Space Technol. 59 (2016) 215–220, https://doi.org/10.1016/J.TUST.2016.07.016.

[3] Y. Gao, J. Zhang, P. Han, Determination of stress relaxation parameters of concrete in tension at early-age by ring test, Construct. Build. Mater. 41 (2013) 152–164, https://doi.org/10.1016/J.CONBUILDMAT.2012.12.004.

[4] V. Semianiuk, V. Tur, M.F. Herrador, M. Paredes G., Early age strains and self-stresses of expansive concrete members under uniaxial restraint conditions, Construct. Build. Mater. 131 (2017) 39–49, https://doi.org/10.1016/J.CONBUILDMAT.2016.11.008.

[5] A.E. Klausen, T. Kanstad, Ø. Bjøntegaard, Hardening concrete exposed to realistic curing temperature regimes and restraint conditions: advanced testing and design methodology, Adv. Mater. Sci. Eng. 2019 (2019), https://doi.org/10.1155/2019/9071034.

[6] D. Shen, J. Jiang, J. Shen, P. Yao, G. Jiang, Influence of curing temperature on autogenous shrinkage and cracking resistance of high-performance concrete at an early age, Construct. Build. Mater. 103 (2016) 67–76, https://doi.org/10.1016/J.CONBUILDMAT.2015.11.039.

[7] J. Xin, G. Zhang, Y. Liu, Z. Wang, Z. Wu, Evaluation of behavior and cracking potential of early-age cementitious systems using uniaxial restraint tests: a review, Construct. Build. Mater. 231 (2020) 117146, https://doi.org/10.1016/J.CONBUILDMAT.2019.117146.

[8] Z. Li, T. Lu, X. Liang, H. Dong, G. Ye, Mechanisms of autogenous shrinkage of alkali-activated slag and fly ash pastes, Cement Concr. Res. 135 (2020), https://doi.org/10.1016/j.cemconres.2020.106107.

[9] M. Liang, Z. Li, S. He, Z. Chang, Y. Gan, E. Schlangen, B. Šavija, Stress evolution in restrained GGBFS concrete due to autogenous deformation: bayesian optimization of aging creep, Construct. Build. Mater. 324 (2022) 126690, https://doi.org/10.1016/J.CONBUILDMAT.2022.126690.

[10] M. Liang, Z. Chang, S. He, Y. Chen, Y. Gan, E. Schlangen, B. Šavija, Predicting early-age stress evolution in restrained concrete by thermo-chemo-mechanical model and active ensemble learning, Comput. Aided Civ. Infrastruct. Eng. 37 (2022) 1809–1833, https://doi.org/10.1111/mice.12915.

[11] G. di Luzio, G. Cusatis, Hygro-thermo-chemical modeling of high-performance concrete. II: numerical implementation, calibration, and validation, Cem. Concr. Compos. 31 (2009) 309–324, https://doi.org/10.1016/J.CEMCONCOMP.2009.02.016.

[12] G. di Luzio, G. Cusatis, Hygro-thermo-chemical modeling of high performance concrete. I: theory, Cem. Concr. Compos. 31 (2009) 301–308, https://doi.org/10.1016/J.CEMCONCOMP.2009.02.015.

[13] M. Liang, Z. Chang, Y. Zhang, H. Cheng, S. He, E. Schlangen, B. Šavija, Autogenous deformation induced- stress evolution in high-volume GGBFS concrete: macro-scale behavior and micro-scale origin, Construct. Build. Mater. 370 (2023) 130663, https://doi.org/10.1016/j.conbuildmat.2023.130663.

[14] S.J. Lokhorst, Deformational Behaviour of Concrete Influenced by Hydration Related Changes of the Microstructure, Delft University of Technology, 2001.

[15] R. Springenschmid, R. Breitenbücher, M. Mangold, Development of the cracking frame and the temperature-stress testing machine, in: Proceedings of the International RILEM Symposium, 1994, pp. 137–144. Munich, Germany.

[16] S. Igarashi, A. Bentur, K. Kovler, Autogenous shrinkage and induced restraining stresses in high-strength concretes, Cement Concr. Res. 30 (2000) 1701–1707, https://doi.org/10.1016/S0008-8846(00)00399-9.

[17] Ø. Bjøntegaard, Termal Dilation and Autogenous Deformation as Driving Forces to Self-Induced Stresses in High Performance Concrete, Norwegian University of Science and Technology (NTNU), 1999. Ph.D. thesis.

[18] A.E. Klausen, Early Age Crack Assessment of Concrete Structures, Experimental Determination of Decisive Parameters, NTNU, 2016. Ph.D. thesis.

[19] D.H. Nguyen, V.T. Nguyen, P. Lura, V.T.N. Dao, Temperature-stress testing machine – a state-of-the-art design and its unique applications in concrete research, Cem. Concr. Compos. 102 (2019) 28–38, https://doi.org/10.1016/J.CEMCONCOMP.2019.04.019.

[20] G. Ou, Z. Lin, T. Kishi, The practical application of a self-developed temperature stress testing machine in development of expansive concrete blended with calcium sulfoaluminate additives, Cement Concr. Res. 164 (2023) 107045, https://doi.org/10.1016/j.cemconres.2022.107045.

[21] S. Staquet, B. Delsaute, A. Darquennes, B. Espion, Design of a revisited TSTM system for testing concrete since setting time under free and restraint conditions, in: CONCRACK 3 – RILEM-JCI International Workshop on Crack Control of Mass Concrete and Related Issues Concerning Early-Age of Concrete Structures, 2012. Paris, France.

[22] B. Delsaute, C. Boulay, S. Staquet, Creep testing of concrete since setting time by means of permanent and repeated minute-long loadings, Cem. Concr. Compos. 73 (2016) 75–88, https://doi.org/10.1016/J.CEMCONCOMP.2016.07.005.

[23] M. Irfan-ul-Hassan, B. Pichler, R. Reihsner, Ch Hellmich, Elastic and creep properties of young cement paste, as determined from hourly repeated minute-long quasi-static tests, Cement Concr. Res. 82 (2016) 36–49, https://doi.org/10.1016/j.cemconres.2015.11.007.

[24] P. Gao, G. Ye, H. Huang, Z. Qian, E. Schlangen, J. Wei, Q. Yu, Incorporating elastic and creep deformations in modelling the three-dimensional autogenous shrinkage of cement paste, Cement Concr. Res. 160 (2022) 106907, https://doi.org/10.1016/J.CEMCONRES.2022.106907.

[25] T. Lu, Z. Li, H. Huang, Restraining effect of aggregates on autogenous shrinkage in cement mortar and concrete, Construct. Build. Mater. 289 (2021) 123166, https://doi.org/10.1016/J.CONBUILDMAT.2021.123166.

[26] T. Lu, Z. Li, H. Huang, Effect of supplementary materials on the autogenous shrinkage of cement paste, Materials 13 (2020) 1–15, https://doi.org/10.3390/ma13153367.

[27] T. Lu, Z. Li, K. van Breugel, Modelling of autogenous shrinkage of hardening cement paste, Construct. Build. Mater. 264 (2020), https://doi.org/10.1016/j.conbuildmat.2020.120708.

[28] Z. Li, T. Lu, Y. Chen, B. Wu, G. Ye, Prediction of the autogenous shrinkage and microcracking of alkali-activated slag and fly ash concrete, Cem. Concr. Compos. 117 (2021), https://doi.org/10.1016/j.cemconcomp.2020.103913.

[29] A.A. Chiniforush, M. Gharehchaei, A. Akbar Nezhad, A. Castel, F. Moghaddam, L. Keyte, D. Hocking, S. Foster, Numerical simulation of risk mitigation strategies for early-age thermal cracking and DEF in concrete, Construct. Build. Mater. 322 (2022) 126478, https://doi.org/10.1016/J.CONBUILDMAT.2022.126478.

[30] D. Gawin, F. Pesavento, B.A. Schrefler, Hygro-thermo-chemo-mechanical modelling of concrete at early ages and beyond. Part I: hydration and hygro-thermal phenomena, Int. J. Numer. Methods Eng. 67 (2006) 299–331, https://doi.org/10.1002/nme.1615.

[31] P. Gao, Y. Chen, H. Huang, Z. Qian, E. Schlangen, J. Wei, Q. Yu, Effect of coarse aggregate size on non-uniform stress/strain and drying-induced microcracking in concrete, Compos. B Eng. 216 (2021), https://doi.org/10.1016/j.compositesb.2021.108880.

[32] B. Klemczak, A. Żmij, Reliability of standard methods for evaluating the early-age cracking risk of thermal-shrinkage origin in concrete walls, Construct. Build. Mater. 226 (2019) 651–661, https://doi.org/10.1016/j.conbuildmat.2019.07.167.

[33] J.R. van Bokhorst, Early-age cracking of concrete A study into the influence of stress relaxation on early-age cracking of concrete structures under imposed deformations, n.d. http://repository.tudelft.nl/.

[34] Y. Gao, J. Zhang, P. Han, Determination of stress relaxation parameters of concrete in tension at early-age by ring test, Construct. Build. Mater. 41 (2013) 152–164, https://doi.org/10.1016/j.conbuildmat.2012.12.004.

[35] M. Azenha, F. Kanavaris, D. Schlicke, A. Jędrzejewska, F. Benboudjema, T. Honorio, V. Šmilauer, C. Serra, J. Forth, K. Riding, B. Khadka, C. Sousa, M. Briffaut, L. Lacarrière, E. Koenders, T. Kanstad, A. Klausen, J.M. Torrenti, E.M. R. Fairbairn, Recommendations of RILEM TC 287-CCS: thermo-chemo-mechanical modelling of massive concrete structures towards cracking risk assessment, Materials and Structures/Materiaux et Constructions 54 (2021) 135, https://doi.org/10.1617/s11527-021-01732-8.

[36] Z.P. Bažant, M. Jirásek, Creep and Hygrothermal Effects in Concrete Structures, Springer Netherlands, Dordrecht, 2018, https://doi.org/10.1007/978-94-024-1138-6.

[37] Z.P. Bazant, E. Osman, Double power law for basic creep of concrete, in: Matériaux et Construction, 9, 1976.

[38] F. Wittmann, Bestimmung physikalischer Eigenschaften des Zementsteins, 1974.

[39] K. Van Breugel, Relaxation of Young Concrete, 1980.

[40] Z. Li, S. Zhang, X. Liang, G. Ye, Cracking potential of alkali-activated slag and fly ash concrete subjected to restrained autogenous shrinkage, Cem. Concr. Compos. 114 (2020), https://doi.org/10.1016/j.cemconcomp.2020.103767.

[41] M. Wyrzykowski, Z. Hu, S. Ghourchian, K. Scrivener, P. Lura, Corrugated tube protocol for autogenous shrinkage measurements: review and statistical assessment, Mater. Struct. 50 (2017) 57, https://doi.org/10.1617/s11527-016-0933-2.

[42] M. Liang, Z. Chang, Z. Wan, Y. Gan, E. Schlangen, B. Šavija, Interpretable Ensemble-Machine-Learning models for predicting creep behavior of concrete, Cem. Concr. Compos. 125 (2022) 104295, https://doi.org/10.1016/J.CEMCONCOMP.2021.104295.

[43] M. Liang, Y. Gan, Z. Chang, Z. Wan, E. Schlangen, B. Šavija, Microstructure-informed deep convolutional neural network for predicting short-term creep modulus of cement paste, Cement Concr. Res. 152 (2022) 106681, https://doi.org/10.1016/J.CEMCONRES.2021.106681.

[44] P. Lura, O.M. Jensen, J. Weiss, Cracking in cement paste induced by autogenous shrinkage, Materials and Structures/Materiaux et Constructions, 42, 2009, pp. 1089–1099, https://doi.org/10.1617/s11527-008-9445-z.

[45] L. Wu, N. Farzadnia, C. Shi, Z. Zhang, H. Wang, Autogenous shrinkage of high performance concrete: a review, Construct. Build. Mater. 149 (2017) 62–75, https://doi.org/10.1016/j.conbuildmat.2017.05.064.

[46] K.M. Lee, H.K. Lee, S.H. Lee, G.Y. Kim, Autogenous shrinkage of concrete containing granulated blast-furnace slag, Cement Concr. Res. 36 (2006) 1279–1285, https://doi.org/10.1016/J.CEMCONRES.2006.01.005.

[47] P. Virtanen, R. Gommers, T.E. Oliphant, M. Haberland, T. Reddy, D. Cournapeau, E. Burovski, P. Peterson, W. Weckesser, J. Bright, S.J. van der Walt, M. Brett, J. Wilson, K.J. Millman, N. Mayorov, A.R.J. Nelson, E. Jones, R. Kern, E. Larson, C. J. Carey, İ. Polat, Y. Feng, E.W. Moore, J. VanderPlas, D. Laxalde, J. Perktold, R. Cimrman, I. Henriksen, E.A. Quintero, C.R. Harris, A.M. Archibald, A.H. Ribeiro, F. Pedregosa, P. van Mulbregt, A. Vijaykumar, A. pietro Bardelli, A. Rothberg, A. Hilboll, A. Kloeckner, A. Scopatz, A. Lee, A. Rokem, C.N. Woods, C. Fulton, C. Masson, C. Häggström, C. Fitzgerald, D.A. Nicholson, D.R. Hagen, D. v. Pasechnik, E. Olivetti, E. Martin, E. Wieser, F. Silva, F. Lenders, F. Wilhelm, G. Young, G.A. Price, G.-L. Ingold, G.E. Allen, G.R. Lee, H. Audren, I. Probst, J. P. Dietrich, J. Silterra, J.T. Webber, J. Slavič, J. Nothman, J. Buchner, J. Kulick, J. L. Schönberger, J.V. de Miranda Cardoso, J. Reimer, J. Harrington, J.L. C. Rodríguez, J. Nunez-Iglesias, J. Kuczynski, K. Tritz, M. Thoma, M. Newville, M. Kümmerer, M. Bolingbroke, M. Tartre, M. Pak, N.J. Smith, N. Nowaczyk, N. Shebanov, O. Pavlyk, P.A. Brodtkorb, P. Lee, R.T. McGibbon, R. Feldbauer,

S. Lewis, S. Tygier, S. Sievert, S. Vigna, S. Peterson, S. More, T. Pudlik, T. Oshima, T.J. Pingel, T.P. Robitaille, T. Spura, T.R. Jones, T. Cera, T. Leslie, T. Zito, T. Krauss, U. Upadhyay, Y.O. Halchenko, Y. Vázquez-Baeza, SciPy 1.0: fundamental algorithms for scientific computing in Python, Nat. Methods 17 (2020) 261–272, https://doi.org/10.1038/s41592-019-0686-2.